PNAS

Supporting Information for

Evolution of genome-wide barriers to gene flow during complex speciation in rattlesnakes

Keaka Farleigh[1], Dylan K. Highland[1], Megan G. Alderman[1], Yannick Francioli[2], Samuel R. Hirst[3], Ellie M. Faber[1], Blair W. Perry[4], Matthew L. Holding[5,6], Gamaliel Castañeda-Gaytán[7], Miguel Borja[7], Hector Franz-Chávez[8], Christopher L. Parkinson[9], Jason L. Strickland[10], Mark J. Margres[3], Stephen P. Mackessy[11], Jesse M. Meik[12], Todd A. Castoe[2], and Drew R. Schield[1,*]

*Corresponding author: Drew R. Schield

Email: drew.schield@virginia.edu

This PDF file includes:

Supporting text
Figures S1 to S23
Tables S1 to S23
SI References

Other supporting materials for this manuscript include the following:

Dataset S1

Supporting Information Text

Genome structure. We examined genome-wide variation in GC content and the density of coding bases ('exon density', measured as the proportion of exon bases in genomic regions; Fig. 2A), finding significantly higher GC content and exon density on microchromosomes than macrochromosomes (Mann-Whitney ∪ tests; *P*-values $< 2.2 \times 10^{-16}$).

Sequencing, mapping, and variant calling. Whole genome sequencing yielded a mean $\pm$ standard deviation of 236 million $\pm$ 126 million 150 bp paired-end reads per sample. A mean of 234.6 million (99.4%) reads mapped to the genome, corresponding to a mean genome-wide read depth of 20.78× per sample. Variant calling resulted in 49,644,347 biallelic SNPs after applying filters, masking female heterozygous sites, and masking repetitive elements. Our final dataset consists of 181 individuals (Fig. 2B), including five species within the Western Rattlesnake species complex (*C. viridis*, *C. concolor*, *C. lutosus*, *C. helleri*, and *C. oreganus*), five species within the Speckled Rattlesnake species complex *sensu lato* (*C. tigris*, *C. stephensi*, *C. pyrrhus*, *C. angelensis*, and *C. mitchellii*), and outgroup species *C. atrox* and *C. ruber* (Table S3).

Phylogeny, population structure, and historical demography. We estimated the phylogeny of the Speckled and Western Rattlesnake species complexes using coalescent species tree and concatenated maximum likelihood approaches, as well as phylogenetic network analysis which relaxes the assumption of a strictly bifurcating topology. We find consistent support across approaches for reciprocal monophyly of the two species complexes, with an inferred common ancestor 4.8 MYA (Fig. 2C; Figs. S1, S2). Our results also strongly support *C. tigris* as sister to the Speckled Rattlesnake complex *sensu stricto*, with an inferred divergence time of 4.2 MYA. Diversification within the Speckled complex occurred from the Late Pliocene through the Pleistocene, and *C. stephensi* is supported as sister to the remaining species complex, including *C. pyrrhus* and *C. mitchellii*, as well as *C. angelensis* and other island endemics in the Gulf of California (*C. polisi* and *C. thalassoporus*; not sampled in this study). Our analyses further indicate that *C. pyrrhus* is paraphyletic with respect to *C. mitchellii*, with *C. mitchellii* being sister to populations of *C. pyrrhus* and *C. angelensis* in mainland Baja California (Fig. 2C; 'Baja 2') and the island of Angel de la Guarda. We recovered two additional clades within *C. pyrrhus*, including populations from Arizona and California and from northern Baja California, respectively. Broadly, our estimated relationships for Speckled Rattlesnakes, including paraphyly of *C. pyrrhus*, agree with previous estimates from Meik et al. (1) and Meik et al. (2). Within the Western complex, we estimate that *C. viridis* and the remaining species diverged ~3.1 MYA, consistent with the divergence time between *C. viridis* and *C. oreganus* estimated in Schield et al. (3). We also find strong support for Mid-Pleistocene divergence between the 'Pacific' clade (including *C. oreganus* and *C. helleri*) and an 'Intermontane' clade (including *C. lutosus* and *C. concolor*), in agreement with estimates from Bernstein et al. (4).

Evidence for the species-level relationships detailed above is largely consistent between tree inference methods and subsets of loci (i.e., genome-wide, autosomes only, or Z chromosome only), albeit with some minor cases of discordance at shallow timescales (Fig. S2). Moreover, phylogenetic network analysis, relaxing the assumption of a bifurcating tree and allowing for reticulation events, reveals evidence for numerous reticulations within and between the species complexes, consistent with a history of introgression during diversification (Fig. 2D; 1, 4–8).

We inferred population genetic structure within the two species complexes using ADMIXTURE and principal component analysis (PCA). ADMIXTURE analysis supported a best-fit model of $K = 10$ genetic clusters (Figs. S1, S3), with lineage-specific ancestry clusters identified for most clades supported by phylogenetic inference (Fig. S1B). We find evidence of finer-scale population structure within *C. viridis* and individual assignment to two ancestry clusters for *C. pyrrhus* from Baja California and within *C. oreganus* and *C. helleri*, potentially due to recent hybridization in these groups. PCA results also clearly distinguish populations within and between the Speckled and Western species complexes (Fig. S4). PC1 explains 31.2% of the variance in genotypes and separates the major species groups. PC2 explains 25.5% of the variance and further separates *C.*

viridis from 'Pacific' and 'Intermontane' species in the Western complex. Inferred changes in effective population size (N_e) through time indicate that current N_e varies widely among species (i.e., 6,000 – 900,000) and that most have experienced expansion or contraction events since the Late Pleistocene (Fig. S6), aligning with previous estimates for a subset of species (9, 10). We infer recent population growth within the Speckled Rattlesnakes, *C. oreganus*, and *C. helleri*, with especially pronounced expansions in *C. mitchellii* and *C. helleri*. By contrast, *C. lutosus*, *C. concolor*, and *C. viridis* have experienced population contractions (Fig. S6). These findings support the hypothesis that species in the temperate Great Plains and Intermontane regions experienced more severe population declines due to climatic fluctuations during the Pleistocene, while species occurring in the warm deserts (especially those in Baja California) were sheltered from these effects, as seen previously in southern *C. ruber* (11).

Evidence for gene flow in secondary contact. Multiple previous studies of the Speckled and Western Rattlesnake species complexes provide evidence for gene flow in secondary contact between divergent populations and species following periods of allopatric divergence (e.g., 1, 4, 5–9, 24). Analyses supporting gene flow in secondary contact include demographic modeling comparing alternative divergence histories, in which models involving secondary contact with gene flow are consistently supported. These tests also strongly reject models of strict allopatric divergence without gene flow. Topology weighting, Patterson's *D* and related tests, coalescent network-based approaches, and cline analyses are also consistent with gene flow in secondary contact in these rattlesnake species complexes, supporting that interpretations of population genetic signatures under a divergence-with-gene-flow model are appropriate in this system.

Materials and Methods

Genome assembly and annotation. All animal procedures in this study were performed using authorized scientific collecting permits and in accordance with animal care and use protocols 2303D-SM-S-26 from University of Northern Colorado and 4482-12-23 from University of Virginia. We sequenced and assembled a reference genome for the Southwestern Speckled Rattlesnake (*Crotalus pyrrhus*) using a combination of PacBio HiFi long-read data and Dovetail Genomics Omni-C chromatin contact data, producing a haplotype-resolved, chromosome-length assembly. We obtained and humanely euthanized a male *C. pyrrhus* from the vicinity of Lake Havasu City, AZ, then prepared snap-frozen tissues for DNA and RNA extraction. High molecular weight DNA was extracted from frozen liver tissue using a PacBio Nanobind PanDNA kit, and we prepared and sequenced a HiFi SMRTbell library on a PacBio Revio targeting 20× coverage per haplotype. We then assembled a draft de novo assembly from the HiFi long-read data using hifiasm (12). We further used extracted DNA from liver tissue to generate an Omni-C library. Briefly, chromatin in the DNA sample was fixed using formaldehyde, and fixed chromatin was digested with DNAse I. Digested chromatin ends were repaired, adapters were ligated, and crosslinks were reversed, then purified DNA was used to produce Illumina libraries, which we sequenced on an Illumina HiSeqX targeting 30× coverage. The *de novo* assembly above was then combined with Omni-C reads for further scaffolding of the assembly using HiRise, a software pipeline designed to incorporate proximity ligation data into scaffold assembly (13). Omni-C reads were mapped to the draft *de novo* assembly prior to analysis in HiRise using BWA (14). We also generated RNA-seq data for liver, heart, blood, testes, venom gland, and accessory venom gland tissues. We mapped RNA-seq data using Bowtie2 (15). We then performed gene prediction and annotation using BRAKERv3.0.8 (16, 17). Finally, we identified repeat elements by mapping known BovB, tetrapod, and snake repeat elements using RepeatMasker v.4.1.7 (18) with default settings. We also used RepeatMasker to identify unknown snake repeats in the *C. pyrrhus* genome.

We used synteny between *C. pyrrhus* and *C. viridis* (19) and *C. adamanteus* (20) to assign scaffolds to chromosomes based on alignments generated using MashMap v3.1.3 (21). We specified a percent identity parameter (--pi) of 95% and segment length parameter (-s) of 50 kb and 10 kb for sequence similarity searches for macrochromosomes and microchromosomes, respectively. We used Python scripts (https://github.com/drewschield/rattlesnake_w_chromosome) to calculate variation in GC content, repeat content, and exon density in sliding windows across the genome.

GC content was calculated as the proportion of 'G' and 'C' nucleotides per window, repeat content was calculated as the proportion of bases in annotated repetitive elements per window, and exon density was calculated as the proportion of bases annotated as exons per window.

Whole genome sequencing and variant calling. We analyzed whole genome sequencing data for 181 *Crotalus* specimens, including 103 samples newly sequenced in this study and 78 from previous studies (3, 4, 6, 10, 22–25), available on NCBI SRA (Table S3). Our sampling includes individual outgroup *C. atrox* and *C. ruber* samples. For new samples, we extracted DNA using a NEB Monarch DNA extraction kit from blood stored in lysis buffer. Illumina Nextera libraries were prepared at the North Texas Genome Center and the University of Oregon GC3F core. Libraries were sequenced on multiple Illumina NovaSeq 6000 S4 lanes using 150 bp paired-end reads, targeting 20× coverage. Following sequencing, we quality filtered reads using Trimmomatic v0.39 (26) with the settings LEADING:20, TRAILING:20, MINLEN:32, and AVGQUAL:30, and mapped filtered reads to the *C. pyrrhus* reference genome using BWA mem v0.7.17-r1188 (14). We used GATK v4.6.1.0-0 and the best practices workflow (27, 28) to call and filter variant sites. We first used GATK HaplotypeCaller to call individual variants, then called variants across the cohort of samples using GATK GenotypeGVCFs to generate an 'all-sites' VCF including data for both variant and invariant sites. We then applied filters to flag low-quality variant calls using GATK VariantFiltration, specifying variance confidence by depth (QD $<$ 2), strand-bias (FS $>$ 60), distance of variant sites from ends of reads (ReadPosRankSum $<$ -8.0), mapping quality of heterozygous sites (MQRankSum $<$ -12.5), and among sample mapping quality (MQ $<$ 40). We masked sites in all individuals where any females had heterozygous calls on the Z chromosome. We also masked sites in repetitive regions and recoded indels and SNPs not passing filters as missing using bcftools v1.10.2 (29).

Phylogeny, population structure, and demography. We estimated the phylogeny of the Speckled and Western Rattlesnake species complexes using multiple approaches, including concatenated maximum likelihood, coalescent species tree inference, and phylogenetic networks to allow for reticulate evolution (SplitsTree App v6.0.0; 30). We performed analysis on three datasets to characterize variation in phylogenetic signal across the genome (4); one including data from all chromosomes, one including only autosomes only, and one including only the Z chromosome. We filtered to retain biallelic SNPs with no missing genotypes among samples. We also thinned to retain one SNP per 10 kb for RaxML analysis to reduce computational burden. We converted VCF data to phylip and nexus files using 'vcf2phylip.py' (https://github.com/edgardomortiz/vcf2phylip) and applied SNP ascertainment bias correction using 'ascbias.py' (https://github.com/btmartin721/raxml_ascbias). We performed maximum likelihood analysis using RaxML-ng v1.2.2 (31, 32) with 100 bootstrap replicates, specifying the GTGTR4+G+ASC_LEWIS model to account for SNP ascertainment bias. We performed coalescent species tree inference using SVDquartets (33), implemented in PAUP v4.0a (34), also with 100 bootstrap replicates. We also used RaxML to calculate branch lengths based on the autosomal SVDquartets topology for estimates of pairwise evolutionary divergence between lineages. Additionally, we relaxed the assumption of a bifurcating tree and allowed for reticulation events using the phylogenetic network method implemented in SplitsTree (30). We calculated genetic distances using 'distMat.py' (https://github.com/simonhmartin/genomics_general/ distMat.py), using the resulting distance matrix as input into the 'Neighbor Net' method (35) implemented in SplitsTree.

We estimated divergence times using treePL v1.0 (36), which employs a penalized likelihood method and calibration dates for specific nodes. We specified three dates in our analysis. Following Bernstein et al. (4), we specified a divergence calibration between *C. atrox* and *C. ruber* with a range of 1.56 – 4.84 MYA (originally estimated in 37). We also used estimated dates from Myers et al. (8) to calibrate the divergence time between the Speckled and Western rattlesnakes (4.8 – 5.1 MYA) and the divergence time between *C. tigris* and the Speckled Rattlesnake complex *sensu stricto* (3.8 – 4.2 MYA). Prior to divergence dating, we determined optimal parameter settings using the 'thorough' and 'prime' functions. We performed cross-validation to determine the smoothing parameter with the lowest error and performed the analysis to estimate divergence dates.

We inferred genetic structure in our dataset using PCA performed in the R package SNPrelate v1.42.0 (38) and model-based ancestry estimation implemented in ADMIXTURE v1.3 (39). We performed analyses after filtering to retain ancestry-informative SNPs with minor allele frequency $\geq$ 0.1. We converted SNP data in VCF format to the input format for ADMIXTURE using PLINK v1.90b6.16 (40). We ran ADMIXTURE under a series of K = 1-15 genetic clusters and determined best-fit model to the data by assessing the model with the lowest cross-validation error (Fig. S3).

We estimated the demographic histories of *Crotalus* species with $n > 1$ using the sequentially Markov coalescent model implemented in SMC++ v1.15.2 (41). Including species with multiple samples provides more robust estimates of effective population size at shallow and deep timescales (42). For analysis of *C. pyrrhus*, we focused on the continental population (see Results). We analyzed biallelic SNPs with < 20% missing genotypes in each species and chose five individuals at random (two for *C. tigris*) to represent 'distinguished' lineages in analysis. We converted autosomal SNPs to SMC++ input format using the 'vcf2smc' function and masked runs of homozygosity >50 kb (-c 50000). We then fit SMC++ models between 1,000 and 200,000 generations in the past using the 'estimate' function, and converted coalescent units to time assuming a per-generation mutation rate of 2.4×10^{-9} (43) and a generation time of 3.3 years (37).

Recombination rate and recombination hotspot identification. We estimated recombination rates in *C. pyrrhus*, *C. stephensi*, *C. viridis*, *C. concolor*, and *C. helleri* using pyrho v0.2.0 (44), which uses composite likelihood to infer the per-generation recombination rate by incorporating an estimate of demographic history. For this, we repeated SMC++ analyses, including only individuals from a single population of each species to avoid the potential for Wahlund effects to affect recombination rate estimates. We used the pyrho 'lookup' function to generate a lookup table based on sample size and inferred demographic history, then used the 'hyperparam' function to evaluate the fit of different block penalty and window size hyperparameters to the data. Based on these analyses, we estimated recombination rates using the 'optimize' function under a block penalty of 20 and window size of 50, and scaled estimates using a mutation rate of 2.4×10^{-9} (43). This procedure occasionally yielded unrealistically high estimates in narrow intervals, which we addressed by masking intervals with rates above the genome-wide 99th percentile in the final recombination map. To examine genome-wide patterns and to compare with other parameters, we calculated mean recombination rate in non-overlapping 1 Mb windows for each species using bedtools v2.29.2 (45). We also calculated mean recombination rate in 1 Mb sliding windows with a 100 kb step for visualization purposes. We evaluated pairwise relationships between recombination landscapes of the different species using Spearman correlation coefficients, revealing significant positive correlations between each pair of species (Fig. S16). Accordingly, we focus primarily on recombination rate variation in *C. pyrrhus*. Nonetheless, we also performed analyses comparing patterns of variation with recombination maps of the other species to verify that the results were consistent regardless of choice of recombination map (Figs. S10, S13).

We identified recombination hotspots following the approaches described in Schield et al. (3) and Hoge et al. (46), with minor adjustments. First, we repeated recombination rate estimation in *C. pyrrhus* using a block penalty of 10, with all other parameters set as before. The rationale for using a lower block penalty is that it increases power to detect fine-scale changes in recombination rate like those seen in hotspots. We then defined hotspots as intervals in the recombination map with a relative recombination rate ('heat') $\geq$5$\times$ that of the mean rate within upstream and downstream 20 kb regions, excluding a 1 kb buffer region centered on the focal interval. Adjacent hotspots within 5 kb of each other were merged. This procedure identified 4,265 hotspots across the *C. pyrrhus* genome with a median length of 1,068 bp. For comparison, we also identified hotspots with a requirement of $\geq$10$\times$ relative heat and repeated these analyses using the recombination map estimated using a block penalty of 20 (Table S7). We defined coldspots as intervals in which the mean recombination rate in 20 kb up- and downstream regions was between 5×10^{-10} and 1.5×10^{-9} and with relative heat between 0.9 and 1.1.

Calculation of introgression and divergence statistics. We examined genome-wide patterns of introgression across scales of divergence by calculating the admixture proportion (f_d), which is proportional to the effective migration rate between populations (47). Calculation of f_d is based on Patterson's *D* (i.e., the 'ABBA-BABA test'; 48), assuming a four-taxon topology ((P1, P2), P3, O), where P1 and P2 are sister, and using an outgroup to distinguish ancestral ('A') from derived ('B') alleles (47). As such, f_d can detect excess derived alleles shared between P2 and P3 ('ABBA' patterns) due to gene flow. We calculated f_d between 13 species pairs in non-overlapping 1 Mb and 100 kb windows (Fig. S6) using 'ABBABABAwindows.py' (https://github.com/simonmartin/genomics_general/), setting *C. atrox* as the outgroup. We retained windows with positive Patterson's *D* and at least 100 informative sites, following recommendations from S. Martin. For analyses between sister species (e.g., *C. lutosus* and *C. concolor*), we assigned samples from distinct populations to P1 and P2 based on our estimated phylogeny, setting the allopatric population more geographically distant from P3 as P1 (Fig. S6).

We estimated absolute divergence (d_{xy}; 49) and relative population differentiation (F_{ST}; 50) in non-overlapping 1 Mb and 100 kb windows using pixy v1.2.3beta1 (51). For visualization purposes, we also calculated f_d, F_{ST}, and d_{xy} in sliding windows with intermediate steps between windows (e.g., 1 Mb windows with a 100 kb step). We compared f_d and F_{ST} distributions across macrochromosomes, microchromosomes, and the Z chromosome using Kruskal-Wallis and pairwise Mann-Whitney U tests. All statistical analyses were performed using R (52).

Distinguishing introgression from incomplete lineage sorting. We tested the possibility that inferred signals of introgression could be generated by incomplete lineage sorting (ILS) alone using permutation analyses of linkage disequilibrium (LD) and absolute sequence divergence (d_{xy}). Under ILS, we expect consistent decreases in LD within high f_d outlier regions relative to the genomic background because recombination will have had longer periods of time to break up haplotypes carrying incompletely sorted ancestral polymorphisms. Conversely, we expect high f_d windows resulting from introgression to exhibit elevated LD because there will have been fewer generations for recombination to break down introgressed haplotypes (although this will depend on the timing and persistence of gene flow). Similarly, under variable rates of ILS across the genome, we would expect regions with extremely low f_d to show reduced d_{xy} because these regions have retained fewer ancestral polymorphisms (47, 53). By contrast, if f_d reflects variable rates of introgression, low f_d regions would be expected to show elevated d_{xy} because they are shielded from gene flow to a greater degree than the rest of the genome. To test these alternatives, we first identified high f_d outlier windows for each species comparison as non-overlapping 1 Mb windows with f_d values greater than any in f_d simulations (see 'Identification of species barriers and fine-scale variation in introgression' section below). We then compared LD in high f_d outliers to the genomic background, controlling for recombination rate and allele frequency differences in empirical outlier windows. We calculated r^2 between SNPs in outlier windows after thinning SNPs by 10 kb using vcftools v0.1.17 (54). We generated genomic backgrounds by limiting the random pool of windows to those with recombination rates within one standard deviation of the mean log-transformed rate and within 5% of mean log-transformed F_{ST} observed in high f_d outlier windows. We randomly selected the same number of windows as empirical outlier windows and calculated mean r^2 for each permutation. We repeated this process 1,000 times to generate a null distribution and compared these to empirical values using Mann-Whitney U tests. We compared dxy patterns in barrier windows (see below) to a recombination rate-controlled genomic background in each species comparison using non-overlapping 1 Mb windows. For each comparison, we generated the genomic background by limiting the random pool of windows to those with recombination rates within one standard deviation of the mean log-transformed rate among barrier windows. We then randomly selected windows equal to the number of barrier windows and calculated mean d_{xy} per window. We repeated this 10,000 times to generate a null distribution and compared these to empirical values using Mann-Whitney U tests.

We do not find consistently reduced LD in high f_d outliers, and find small effect sizes for differences between empirical and background distributions (Fig. S22). Moreover, each empirical distribution contains high f_d outliers with substantially elevated LD, as expected under introgression. Absence

of systematic reduction of LD in high fd outliers suggests that patterns of f_d variation are not driven by ILS alone. Patterns of d_{xy} in barrier windows further suggest that variation in derived allele sharing between non-sister taxa is is not due to ILS alone. Specifically, we find many barrier windows with elevated d_{xy} (Fig. S23), consistent with these regions being shielded from gene flow. Together, these results indicate that, while ILS is likely an ongoing process, genome-wide variation in f_d reflects variation in rates of introgression, and not ILS in the absence of gene flow.

Evolutionary and ecological divergence. We calculated evolutionary and ecological divergence to test whether rates of introgression were associated with different measures of divergence between species. We determined evolutionary divergence using pairwise branch lengths between species estimated using RAxML (see phylogenetic methods above). We derived a composite measure of ecological divergence based on environmental and morphological variables and breeding seasonality. To measure environmental variation, we downloaded occurrences for each species from VertNet (www.vertnet.org) and used terra v1.8-60 (55) to retain occurrences falling within the geographic range of each species. We then extracted environmental data for each occurrence using the WorldClim v2 database (56) at 1 km resolution; these data contain 19 climatic variables related to temperature and precipitation. We thinned occurrences by 10 km using spThin 0.2.0 (57) to avoid potential bias from clusters of nearby occurrences. We then performed PCA to summarize environmental variables across localities and calculated the Mahalanobis distance between species based on the first three principal components. To measure interspecific distance in breeding phenology, we first performed a literature search to determine in which months breeding occurred for each species, then calculated the distance in breeding seasonality as one minus the proportion of breeding season that overlapped between species. We weighted this distance by the length of the breeding season using the formula $1 - ((L_1 po_1 + L_2 po_2)/(L_1 + L_2))$, where L is the breeding season length of each species and po is the proportion of the breeding season each species that overlaps the breeding season of the other. As a measure of morphological distance, we calculated the difference in mean adult body size between species using estimates from a previous study (58) and a body size database collected by JMM from georeferenced field and museum specimens. Finally, we calculated a single ecological divergence measure combining environmental, breeding seasonality, and body size distances as the mean of the three distance measures, after scaling environmental and morphological distance so that the minimum observed values were set to zero and the maximum values were set to one.

Relationships between introgression, recombination, and divergent selection. We tested relationships between introgression, recombination rate, exon density, and population differentiation (F_{ST}) using linear models implemented in R (52). We first calculated Spearman correlation coefficients between f_d and recombination rate, exon density, and F_{ST}, respectively, based on mean values in non-overlapping 1 Mb windows. We further considered the potential interaction between recombination rate and exon density using the formula $f_d \sim rate + density + rate \times density$. We performed partial redundancy analysis using the R package vegan v2.7-1 (59) with recombination rate as a conditioning variable to quantify the amount of variance in f_d explained by exon density and recombination rate, respectively. We further compared f_d distributions in genic and intergenic regions and between recombination hotspots and coldspots using Mann-Whitney U tests based on mean values in non-overlapping 100 kb windows. Intergenic regions were considered windows ≥100 kb from a gene. Finally, we used linear models to test the relationship between fd and exon density while controlling for fine-scale recombination rate variation based on the distance to the nearest hotspot and the recombination rate in the nearest hotspot, using the formula $f_d \sim density + rate + distance$. We then repeated these tests using hotspots identified in the recombination maps of other *Crotalus* species to verify that inferred relationships were not biased by interpretation based on the *C. pyrrhus* map (Fig. S13).

We fit linear and nonlinear models to evaluate broad relationships between the strength of correlation between f_d and recombination rate and evolutionary divergence, and between mean genome-wide f_d and evolutionary and ecological divergence across species pairs, assuming normality of the data (we found no indication that this assumption affected conclusions from these analyses). For the former, we fit linear and quadratic models to the relationship between the

Spearman correlation coefficient between f_d and recombination rate and evolutionary divergence. For the latter, we fit linear and exponential models to the relationship between f_d and evolutionary and ecological divergence, respectively. For each of these, we assessed model fit using the Corrected Akaike Information Criterion (60). We also analyzed fit of these models after performing phylogenetic correction to account for phylogenetic non-independence in comparisons, following (61, 62). We also used linear models to examine the relationships between genome-wide d_{xy} and F_{ST} and ecological divergence. For models comparing the Z chromosome to autosomes, we performed analyses including all macrochromosomes and microchromosomes as well as Chromosome 4, specifically, because it is the autosome most similar in length to the Z chromosome.

Identification of species barriers and fine-scale variation in introgression. We examined relationships between independent f_d landscapes using Spearman correlation coefficients, and evaluated how these correlations change as a function of both mean and minimum evolutionary distance between species pairs. Again, we repeated this analysis correcting for phylogenetic non-independence, following (61, 62). We used a permutation approach to identify outlier barrier windows with lower f_d than observed in the genomic background. For each species pair, we generated simulated windows of equal length as those in empirical comparisons drawn from randomly sampled empirical windows at higher resolution. For example, for each simulated 1 Mb window, we sampled ten 100 kb empirical windows at random. We then calculated mean f_d in each simulated window, repeating random sampling 10,000 times to create simulated null distributions. An empirical window was considered a barrier window if mean f_d in the window fell below the minimum f_d in the null distribution. We then determined if barrier windows were shared across species comparisons and calculated the proportion of species pairs in which a given region constituted a barrier, accounting for missing data for specific windows in some comparisons due to an insufficient number of informative sites or negative *D* values. We used a second permutation approach to determine the proportion of species pairs in which a given barrier window would be expected to appear by chance. First, we randomly selected a number of windows equivalent to the number of windows identified as barriers in each comparison. We then calculated the proportion of comparisons in which each randomly selected window was determined to be a barrier. We repeated this process 10,000 times to generate a null distribution, using the maximum simulated proportion of comparisons sharing a barrier window as the threshold for defining empirical 'shared barriers'. We also repeated this analysis to control for lower recombination rates in barrier windows by limiting the random pool of windows to those with recombination rates within one standard deviation of the mean log-transformed rate among barrier windows. We compared frequencies of species barriers on macrochromosomes, microchromosomes, and the Z chromosome using Kruskal-Wallis and Mann-Whitney U tests, then examined the proportion of each chromosome class annotated as barriers as a function of evolutionary divergence between species using linear models.

We performed gene ontology (GO) analysis in Panther v19.0 (63) to test whether functional categories were overrepresented in shared barrier windows. We extracted all genes in barrier windows that were shared in more than 26% of the comparisons (i.e., the maximum under random expectation) using bedtools 'intersect' (45). We then converted gene names to *Anolis carolinensis* gene IDs (64) for GO analysis. We performed Fisher's exact tests with FDR correction to identify overrepresented biological processes in our list of genes within shared barriers.

We performed bootstrapping to compare rates of introgression in focal regions linked to key adaptive traits (i.e., venom and MHC genes) and overrepresented biological processes from GO analysis of shared barriers to the genome background (e.g., spermatogenesis, oxidative phosphorylation, and chemosensory behavior). For each species pair, we randomly sampled the same number of windows from across the genome as there were in each gene set and calculated mean f_d, repeating this process 10,000 times to generate a null distribution. We tested the hypothesis that candidate genes had higher rates of introgression than the genome background by calculating a *P*-value equal to the proportion of simulated replicates with higher f_d than the median empirical value. To test whether candidate genes involved in biological processes overrepresented in shared barriers had lower rates of introgression than the genome background, we performed the

same procedure, but calculated *P*-values equal to the proportion of simulated replicates with f_d lower than the median empirical value. For comparison, we repeated these analyses, drawing background distributions only from windows containing coding genes. To examine non-redundant gene sets related to overrepresented biological processes, we used ReviGo v1.8.1 (65) with default settings to cluster Panther-identified related GO terms.

Figures

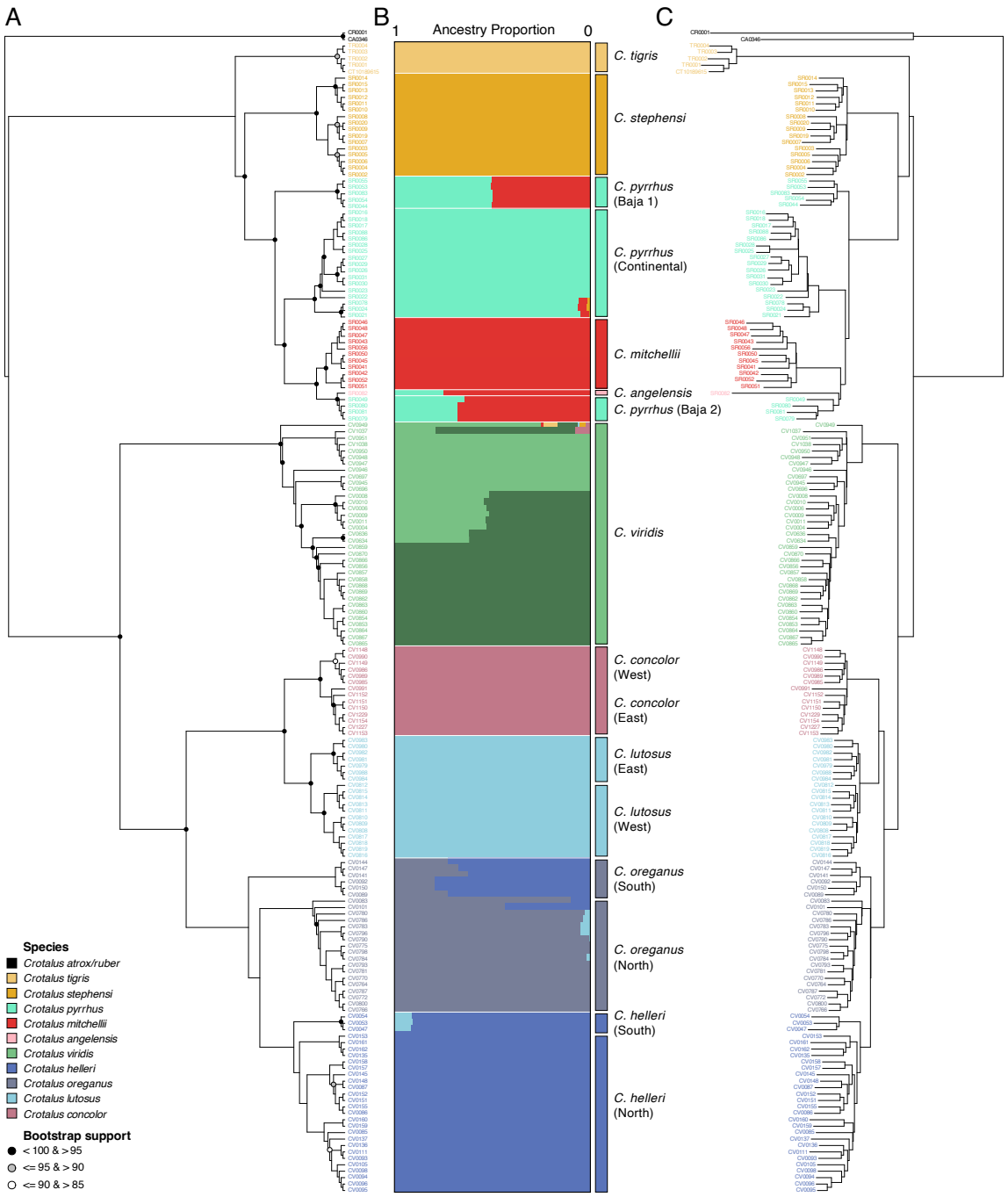

Figure S1. Phylogenetic relationships and population structure among species in the Speckled and Western rattlesnake complexes. **A** Coalescent-based species tree topology estimated from a concatenated matrix of genome-wide SNPs. Individual labels are colored according to species. Circular node labels indicate bootstrap support. **B** Individual ancestry proportions (horizontal bars) between one or more genetic clusters inferred using ADMIXTURE under a $K = 10$ model. Labels to the right of ancestry proportions indicate population subgroups used in introgression analyses. **C** Coalescent species tree topology with branch lengths estimated using RAxML.

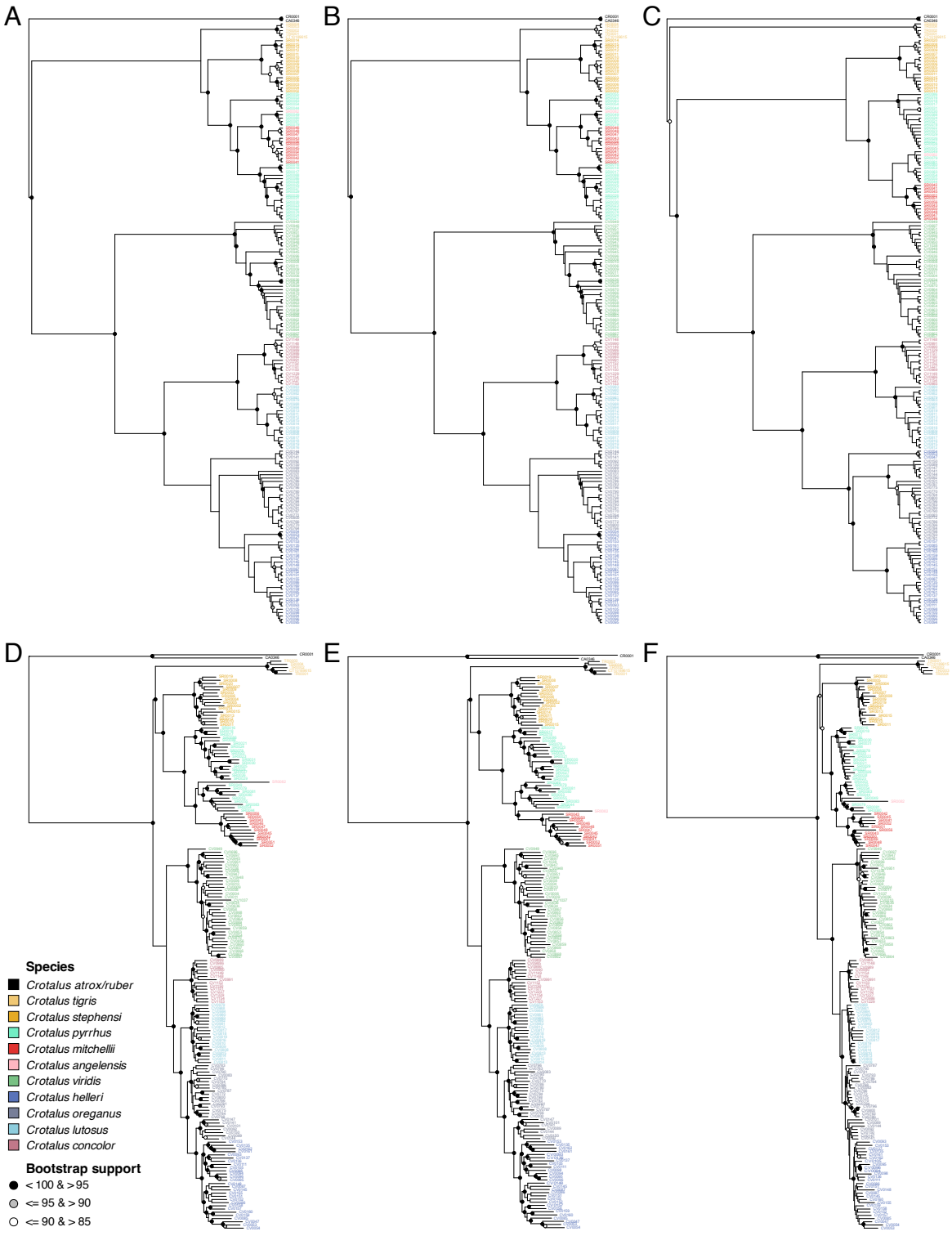

Figure S2. A-C Tree topologies estimated using coalescent-based species tree inference on genome-wide SNPs (**A**), autosomes only (**B**), and the Z chromosome only (**C**). **D-F** Tree topologies estimated using concatenated maximum likelihood on genome-wide SNPs (**D**), autosomes only (**E**), and the Z chromosome only (**F**). Individual labels are colored according to species and circular labels at nodes indicate bootstrap support for relationships.

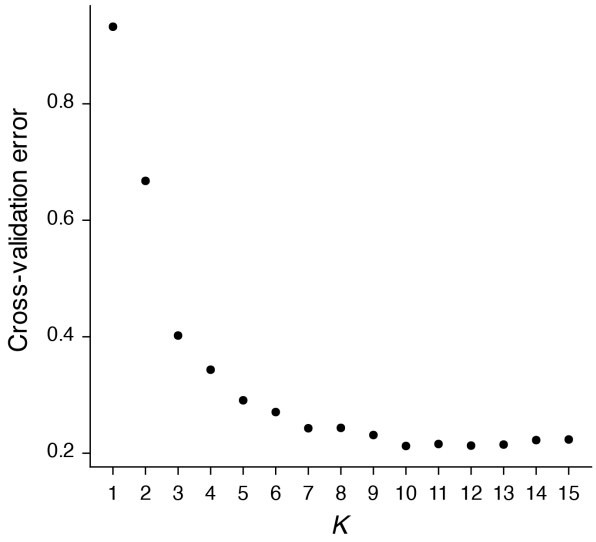

Figure S3. Cross-validation (CV) error across ADMIXTURE analyses for $K = 1$-15 genetic cluster models. The $K = 10$ model had the lowest CV error.

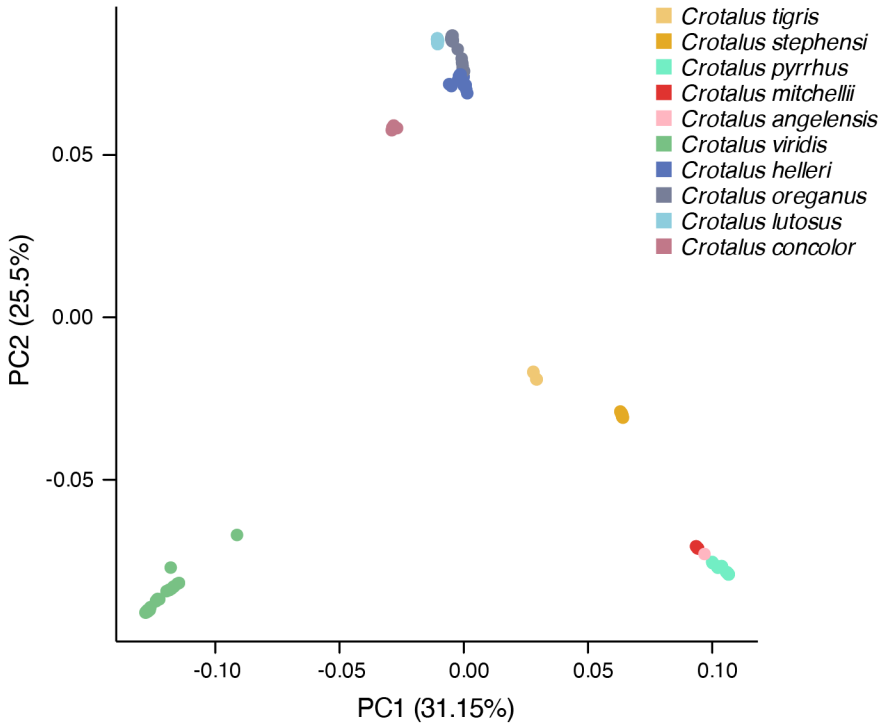

Figure S4. Genetic structure summarized based on principal components PC1 and PC2. Individual points are colored according to species.

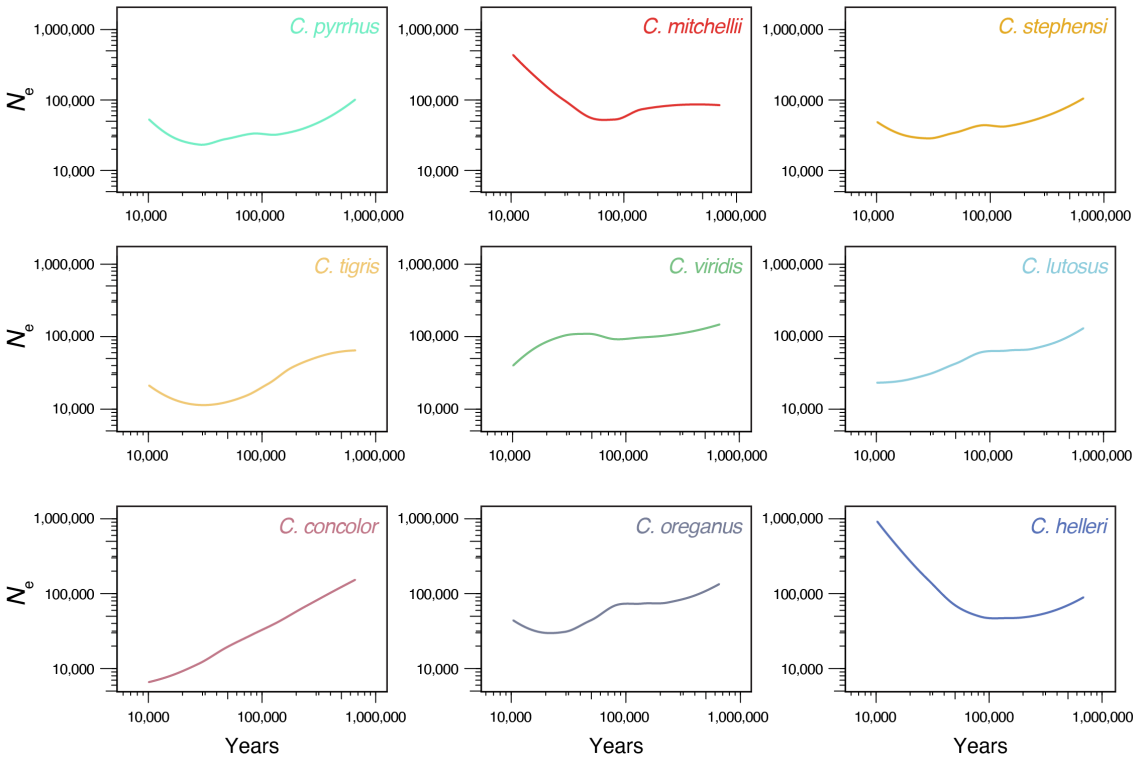

Figure S5. Estimates of changes in effective population size (N_e) over the last 660,000 years for nine *Crotalus* species with $n > 1$ in the current study. Both x-and y-axes are shown on a $\log_{10}$ scale.

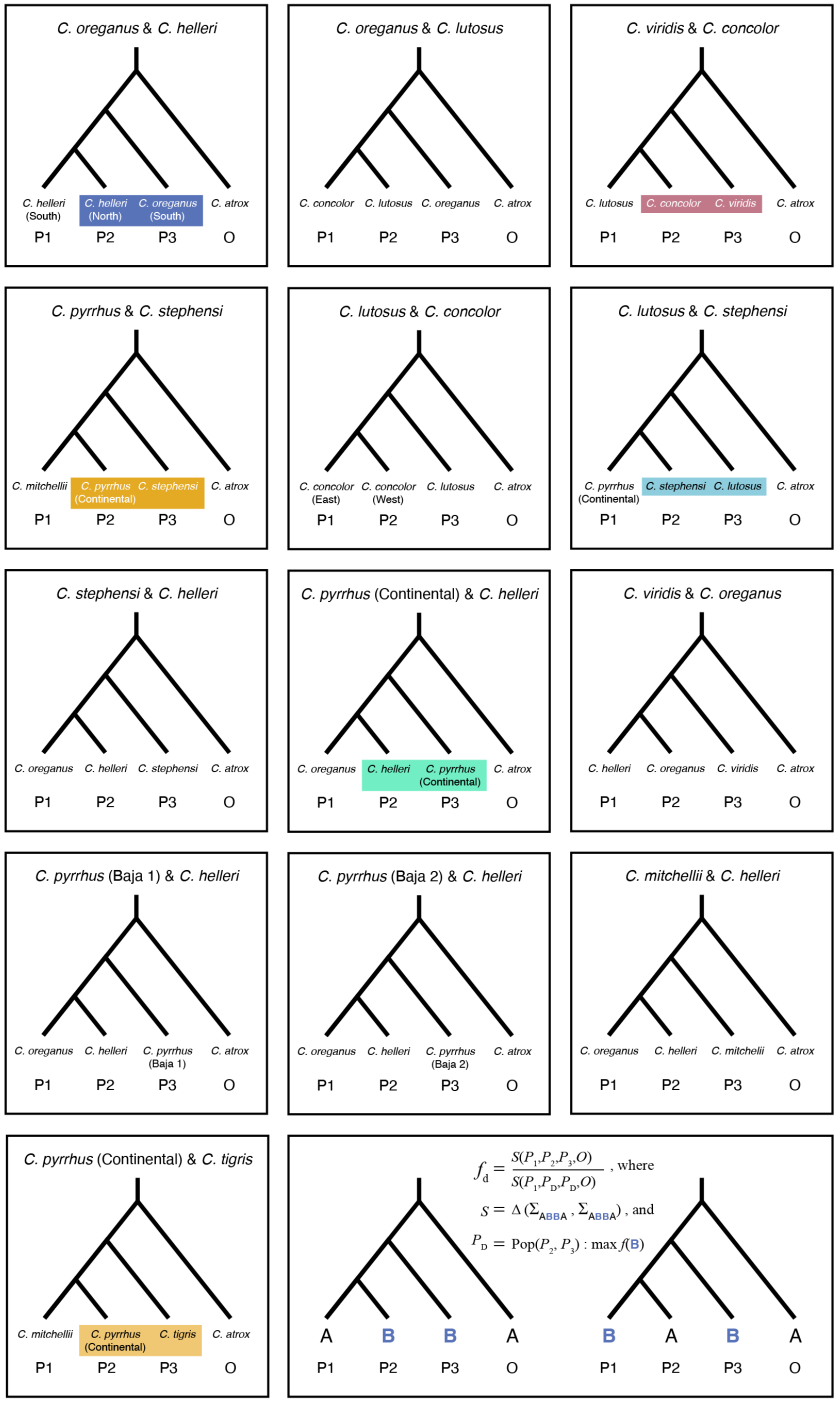

Figure S6. Four-population topologies used to estimate admixture proportions (f_d) between parapatric and sympatric species in the Speckled and Western species complexes. Tests leveraging specific populations within species are noted (e.g., *C. pyrrhus* Continental, *C. pyrrhus* Baja 1, *C. oreganus* North, etc.). Panels with color highlighting P2 and P3 populations match exemplar comparisons in the main text. The bottom right panel shows a schematic of the ABBA-BABA test framework and the f_d formula described in Martin et al. (2015).

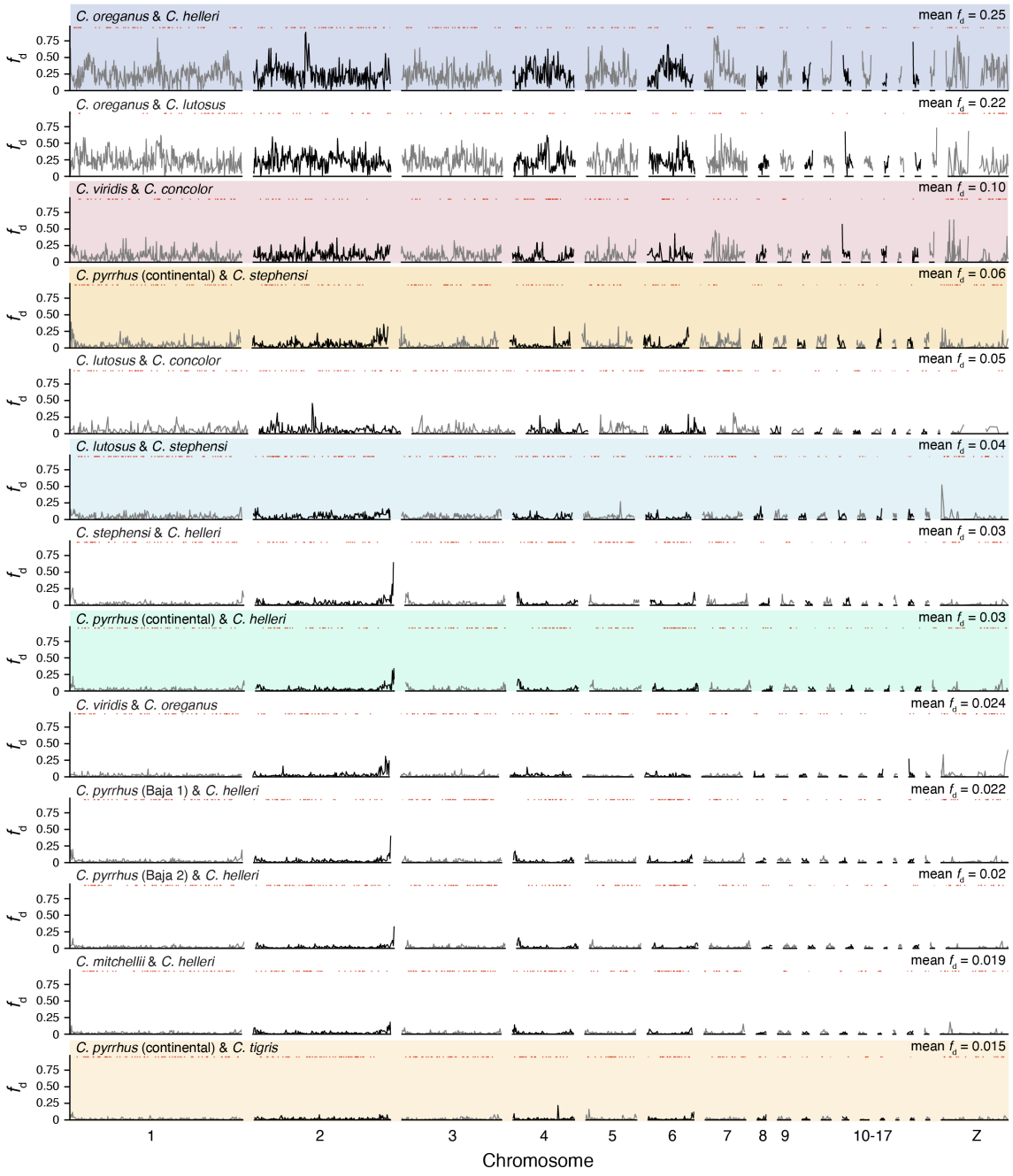

Figure S7. Genomic landscapes of introgression between all pairs of parapatric and sympatric *Crotalus* species analyzed. Genome scans show mean f_d in 1 Mb windows with a 100 kb step between windows. Genome-wide mean f_d for each comparison is indicated at the top right of f_d scans, which are arranged by decreasing f_d from top to bottom. Red dots above scans show locations of inferred barrier loci, as determined by permutation tests. Shaded branches in trees to the left of f_d scans highlight the phylogenetic distance between pairs of species. Color panels match exemplar comparisons in the main text.

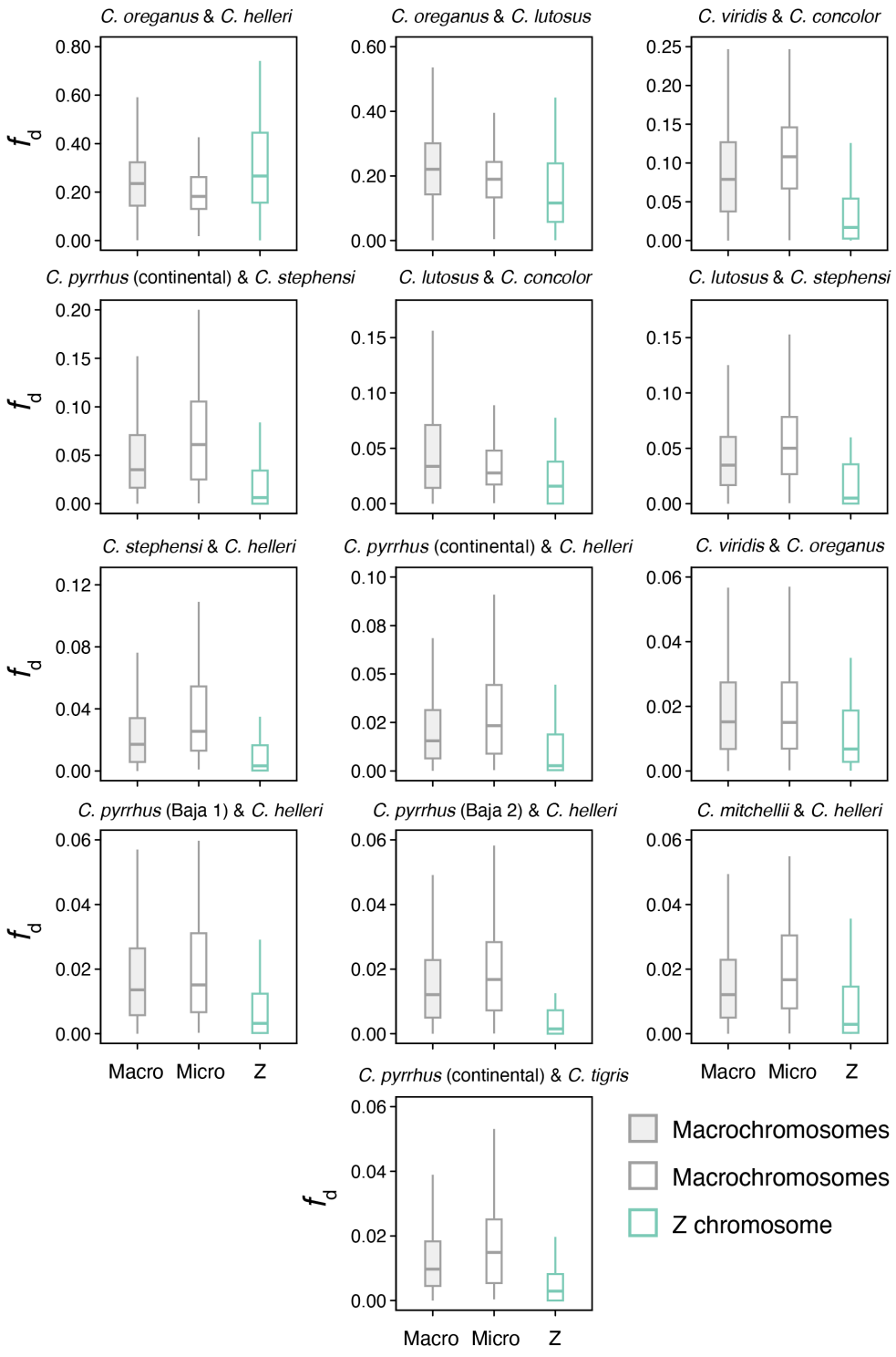

Figure S8. Distributions of f_d on macrochromosomes (filled grey), microchromosomes (open grey), and the Z chromosome (green) between pairs of species. Statistical comparisons of the distributions are provided in Table S5.

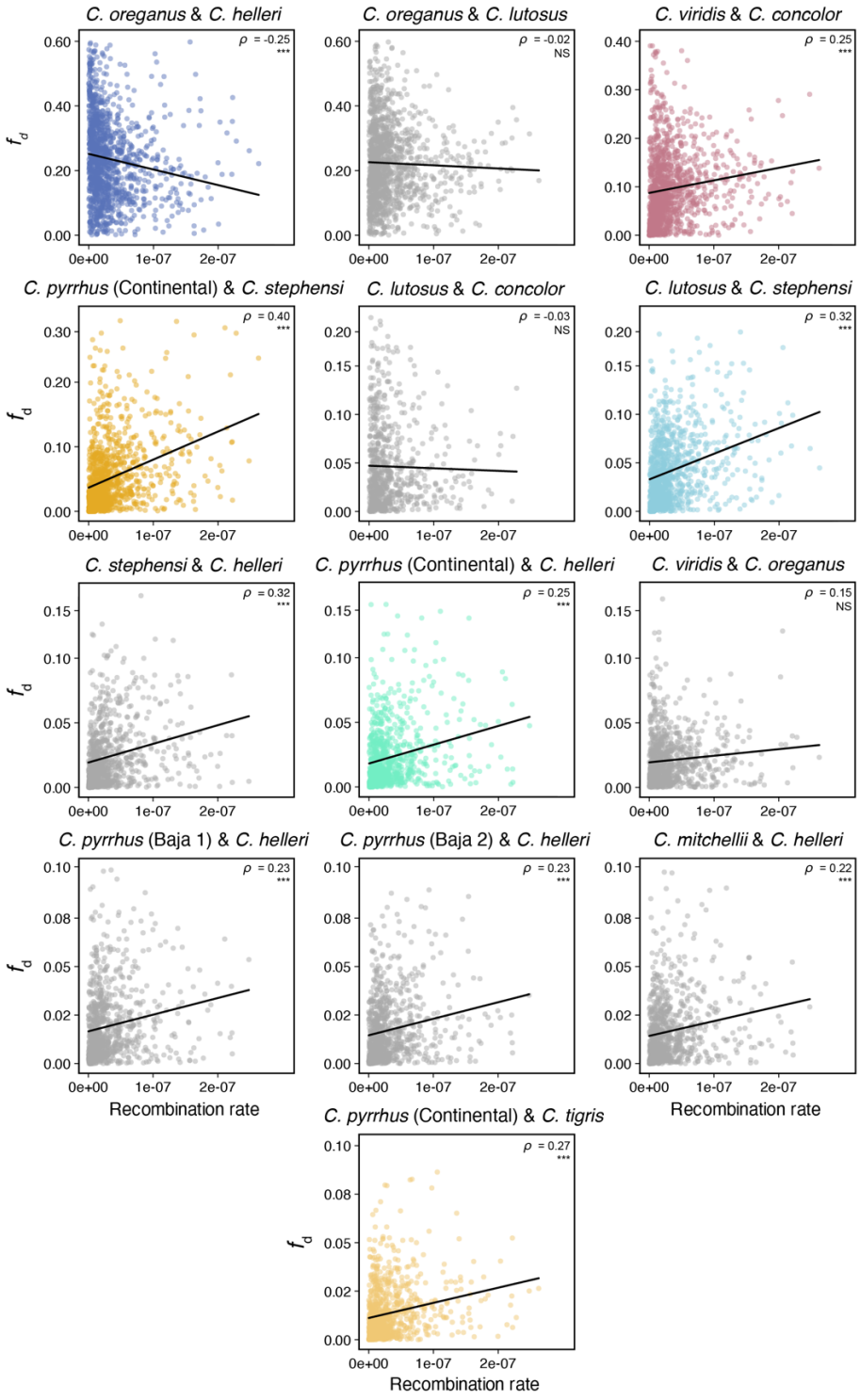

Figure S9. Relationships between genomic landscapes of introgression (f_d) and recombination rate for all species pairs analyzed in the study. Spearman correlation coefficients (ρ) and significance are labeled ($^{***}p < 2.2 \times 10^{-16}$; NS, not significant). All statistical comparisons are based on mean values in non-overlapping 1 Mb windows. Color panels match exemplar comparisons in the main text.

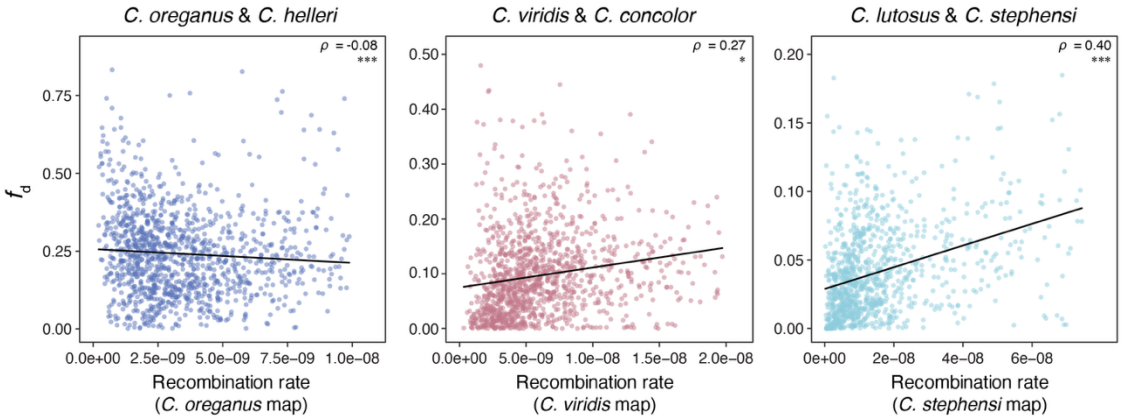

Figure S10. Relationships between f_d and recombination rate, based on recombination landscapes of different species. Shaded points represent mean values in non-overlapping 100 kb windows overlapping each feature. Spearman correlation coefficients are summarized in the top right of each panel. In all panels, $^{***}p < 2.2 \times 10^{-16}$; $^{*}p < 0.05$.

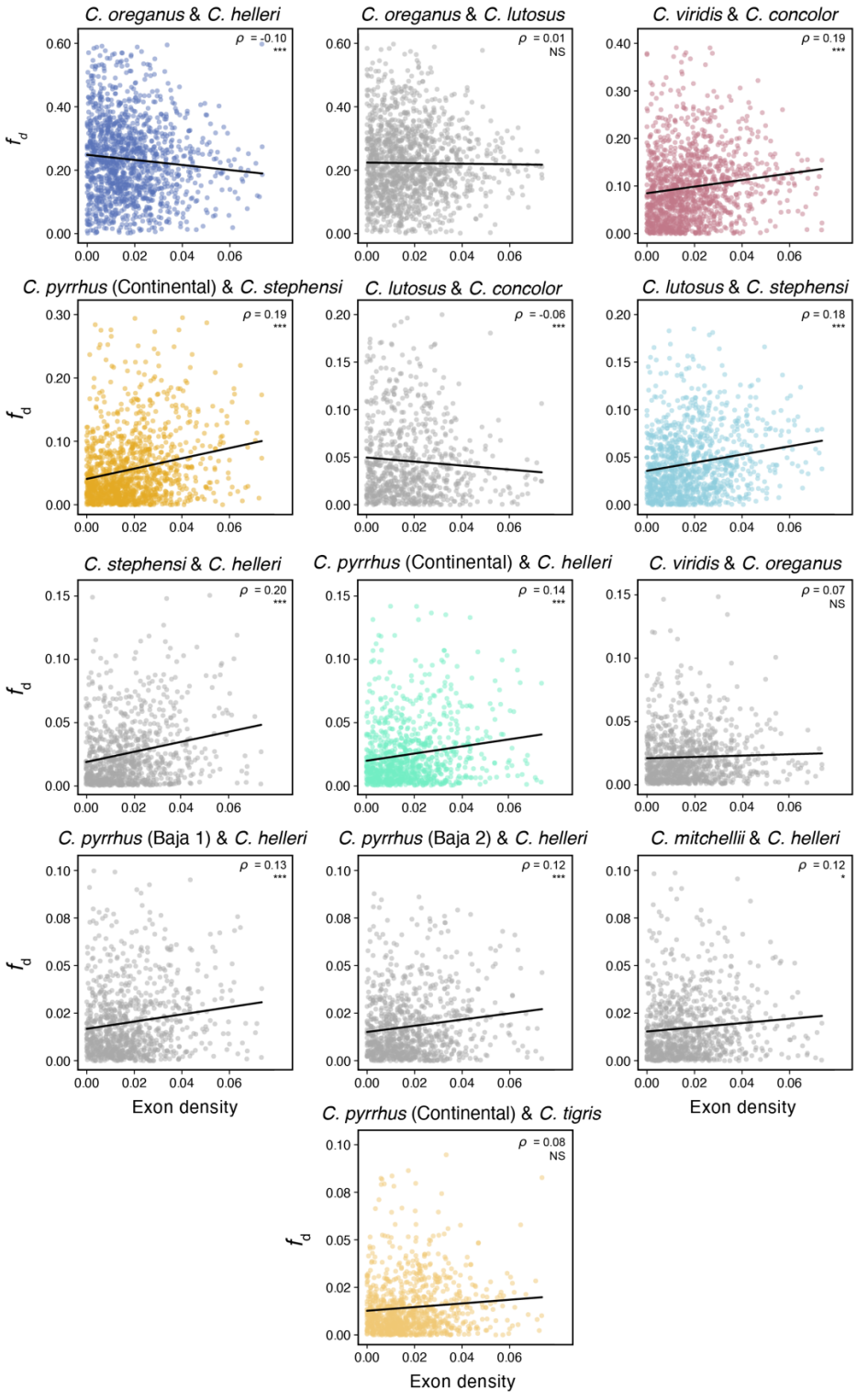

Figure S11. Relationships between genomic landscapes of introgression (f_d) and exon density for all species pairs analyzed in the study. Spearman correlation coefficients (ρ) and significance are labeled ($^{***}p < 2.2 \times 10^{-16}$; NS, not significant). All statistical comparisons are based on mean values in non-overlapping 1 Mb windows. Color panels match exemplar comparisons in the main text.

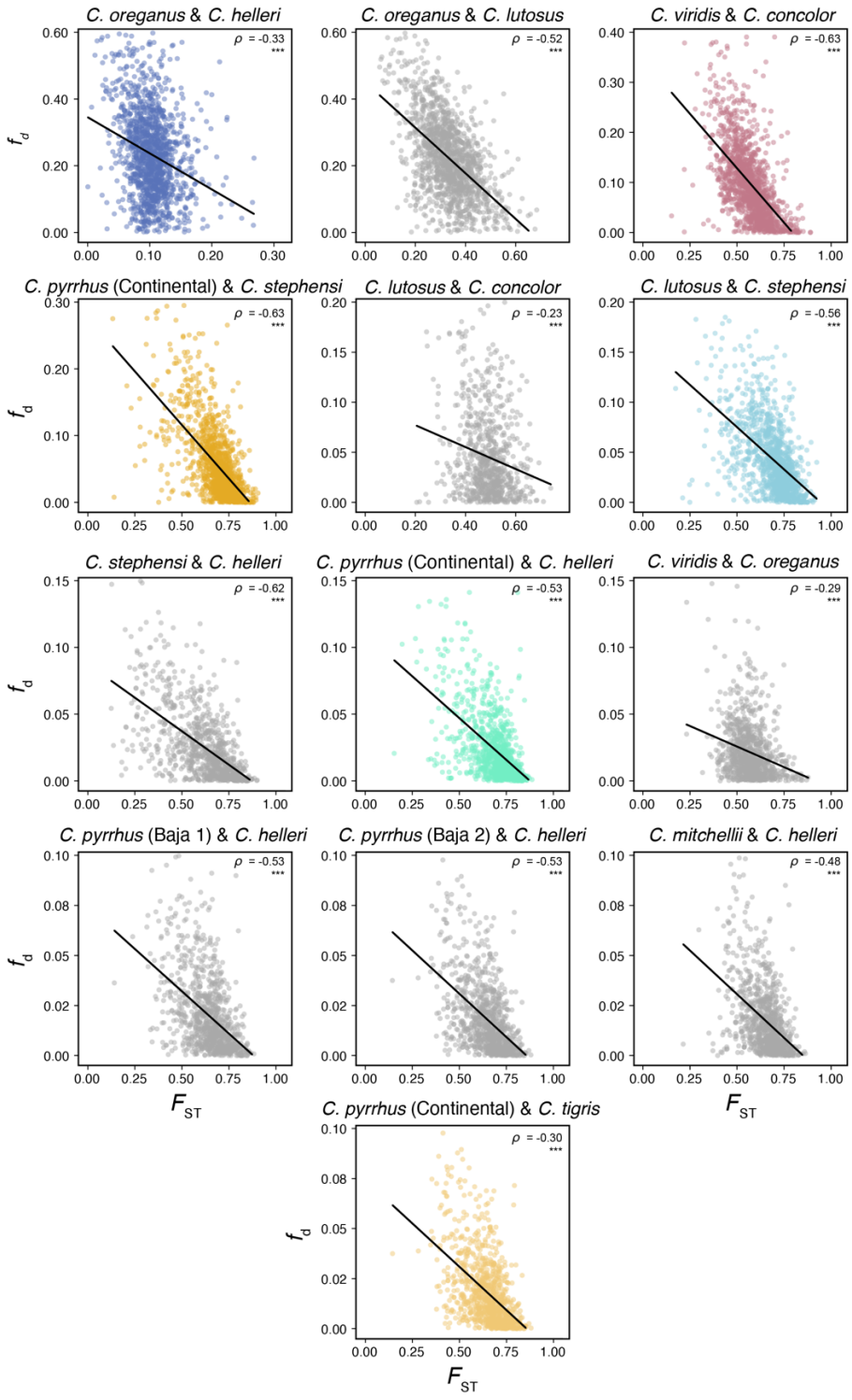

Figure S12. Relationships between genomic landscapes of introgression (f_d) and genetic differentiation (F_{ST}) for all species pairs analyzed in the study. Spearman correlation coefficients (ρ) and significance are labeled ($^{***}p < 2.2 \times 10^{-16}$; NS, not significant). All statistical comparisons are based on mean values in non-overlapping 1 Mb windows. Color panels match exemplar comparisons in the main text.

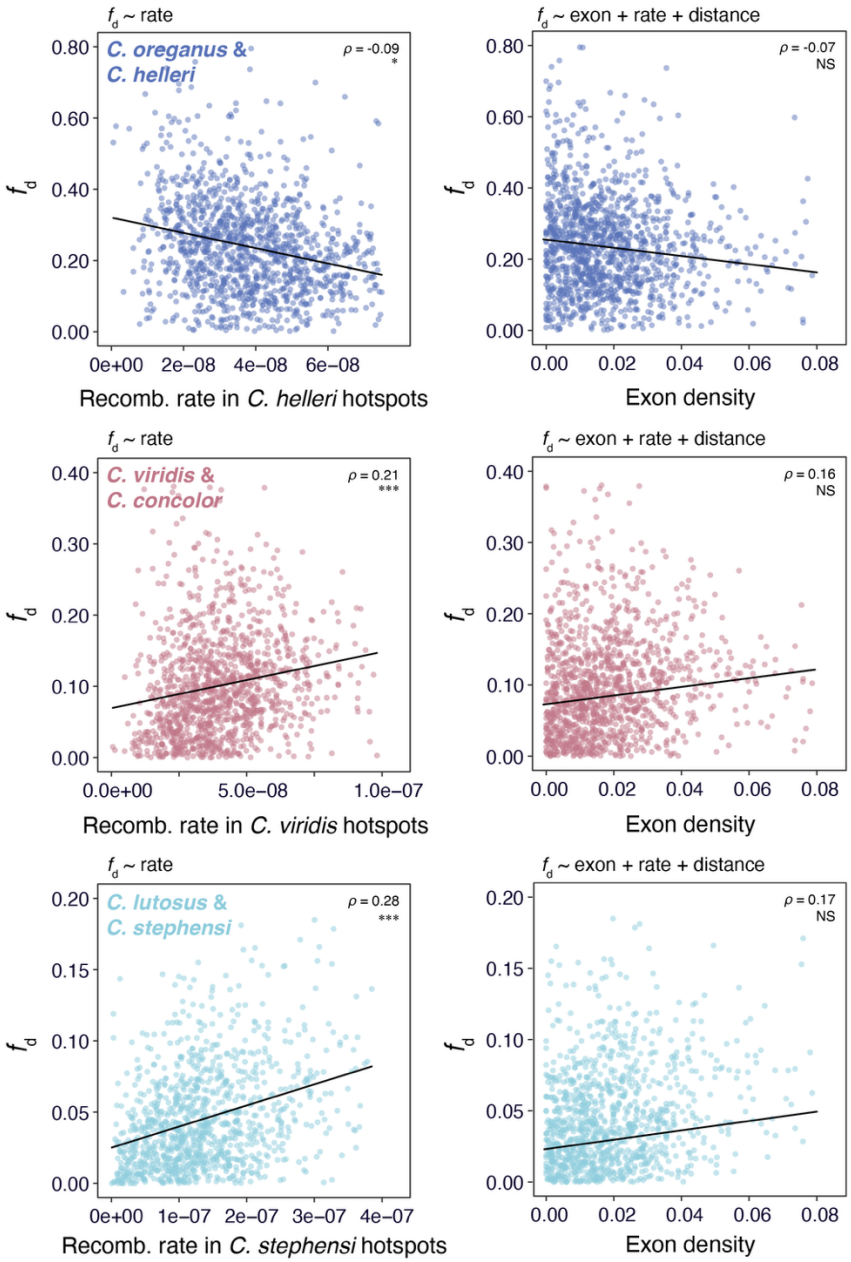

Figure S13. Relationships between f_d and mean recombination rate in hotspot windows for different species (left) and between f_d and exon density in hotspot windows, while controlling for recombination rate in the nearest hotspot and the distance (in bp) to the nearest hotspot (right). Formulas of each linear model are shown above, and Spearman correlation coefficients are summarized in the top right of each panel. Shaded points represent mean values in non-overlapping 100 kb windows overlapping each feature. In all panels, $^{***}p < 2.2 \times 10^{-16}$; NS, not significant.

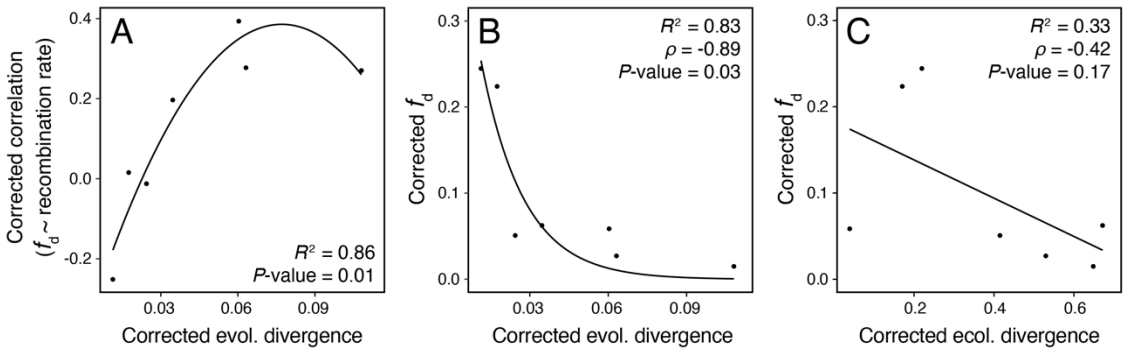

Figure S14. Relationships between f_d ~ recombination correlation and mean f_d with evolutionary and ecological divergence between species, corrected for phylogenetic non-independence. **A** Spearman correlation coefficients between admixture proportions (f_d) and recombination rate as a function of evolutionary divergence. Points are drawn from correlation coefficients calculated from measures in 1 Mb non-overlapping windows. **B** Relationship between mean genome-wide f_d and evolutionary divergence. **C** Relationship between mean genome-wide f_d and ecological divergence. Labels in **A** and **B** summarize Spearman correlation coefficients between f_d and evolutionary and ecological divergence, respectively. Lines in **A**-**C** represent best-fit nonlinear or linear models to the data.

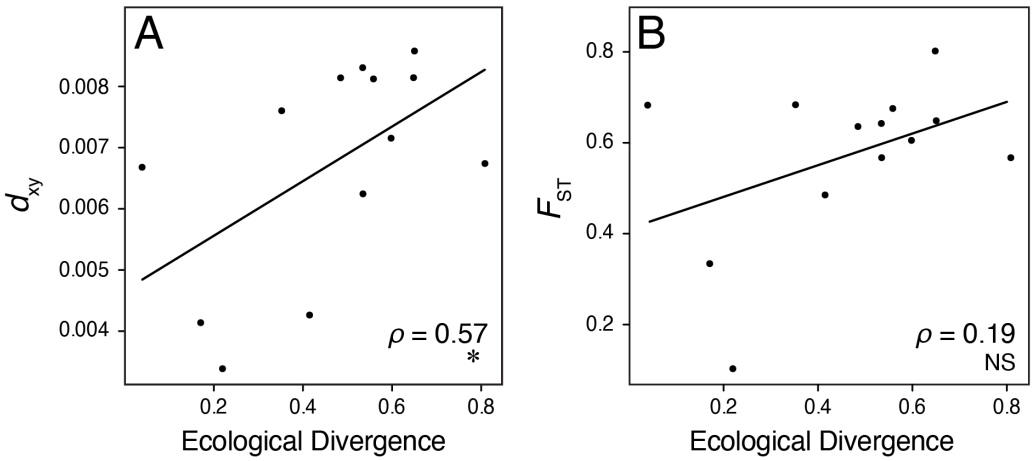

Figure S15. Relationships between ecological divergence and measures of (**A**) absolute genetic divergence (d_{xy}) and (**B**) relative genetic differentiation (F_{ST}) for pairs of parapatric and sympatric *Crotalus* species (points). Spearman correlation coefficients (ρ) and significance are labeled ($^{*}p < 0.05$; NS, not significant).

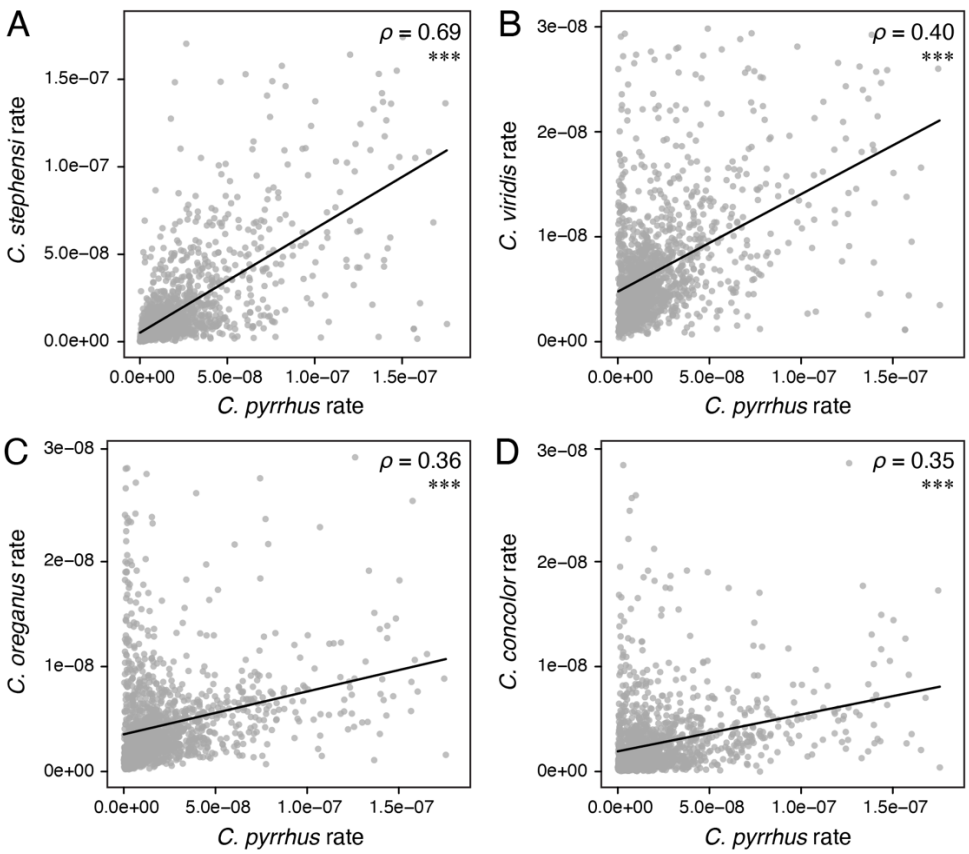

Figure S16. Relationships between recombination landscapes of different *Crotalus* species calculated based on mean recombination rates in non-overlapping 1 Mb windows. Spearman correlation coefficients and significance are indicated in the top right of each panel. In all panels, $^{***}p < 2.2 \times 10^{-16}$.

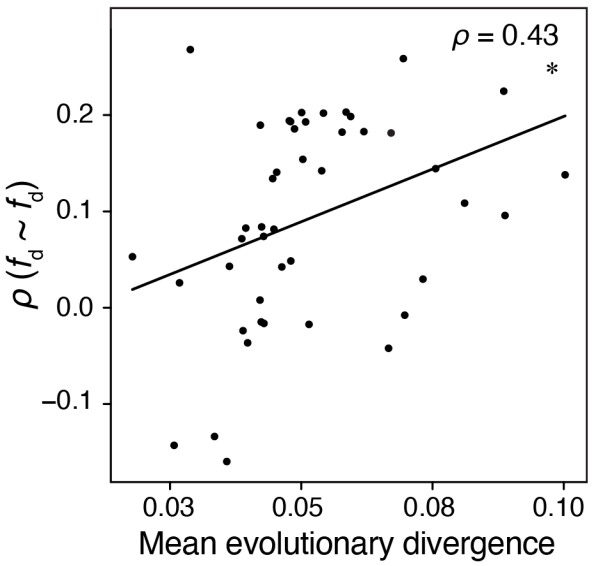

Figure S17. Spearman correlation coefficients (ρ) for genome-wide f_d between all species pairs as a function of the mean evolutionary divergence in each set of species pairs. $^{*}p < 0.05$.

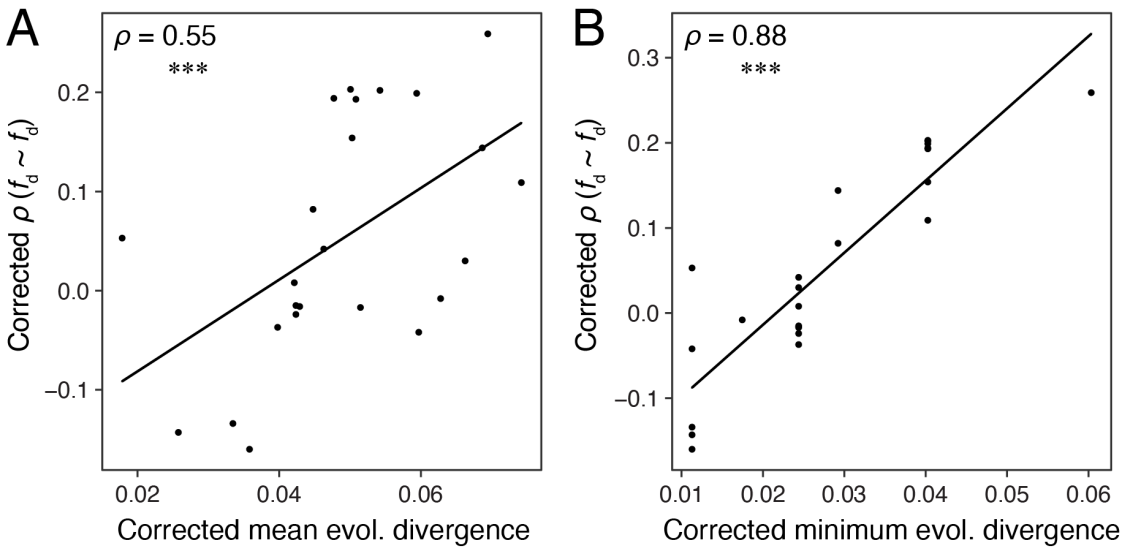

Figure S18. Spearman correlation coefficients (ρ) for genome-wide f_d between all species pairs as a function of the mean (**A**) and minimum (**B**) evolutionary divergence in each set of species pairs, after correcting for phylogenetic non-independence. $^{***}p < 2.2 \times 10^{-16}$.

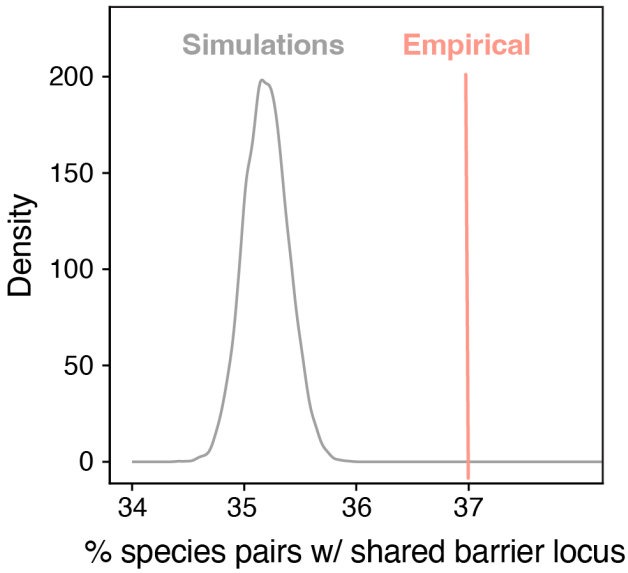

Figure S19. Simulated distribution (grey) of the proportion of species pairs sharing a coincident barrier locus identified between any given pair of species, when controlling for recombination rate by sampling from genomic windows with recombination rate within one standard deviation of the mean recombination rate within barrier loci. The vertical salmon line shows the empirical mean proportion of species pairs sharing barrier loci.

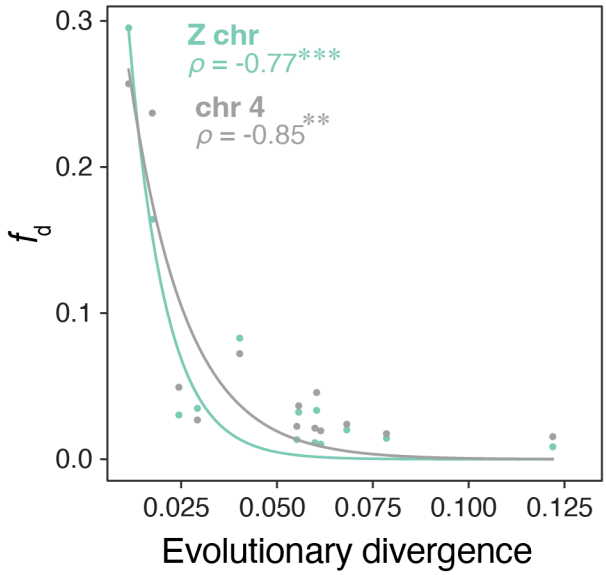

Figure S20. Relationships between mean f_d and evolutionary divergence, with results shown separately for Chromosome 4 (grey points; grey line) and the Z chromosome (green points; green line). $^{***}p < 2.2 \times 10^{-16}$; $^{**}p < 0.001$.

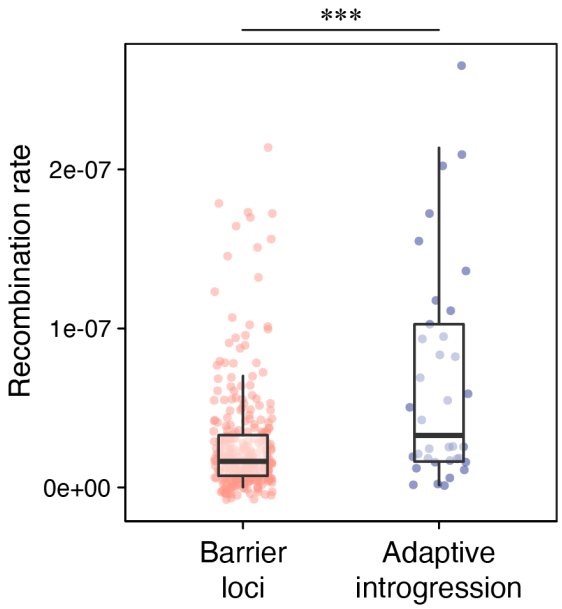

Figure S21. Distributions of recombination rate in barrier loci and putative adaptive introgression loci shown in Fig. 8 of the main text. $^{***}p$-value = 0.0003.

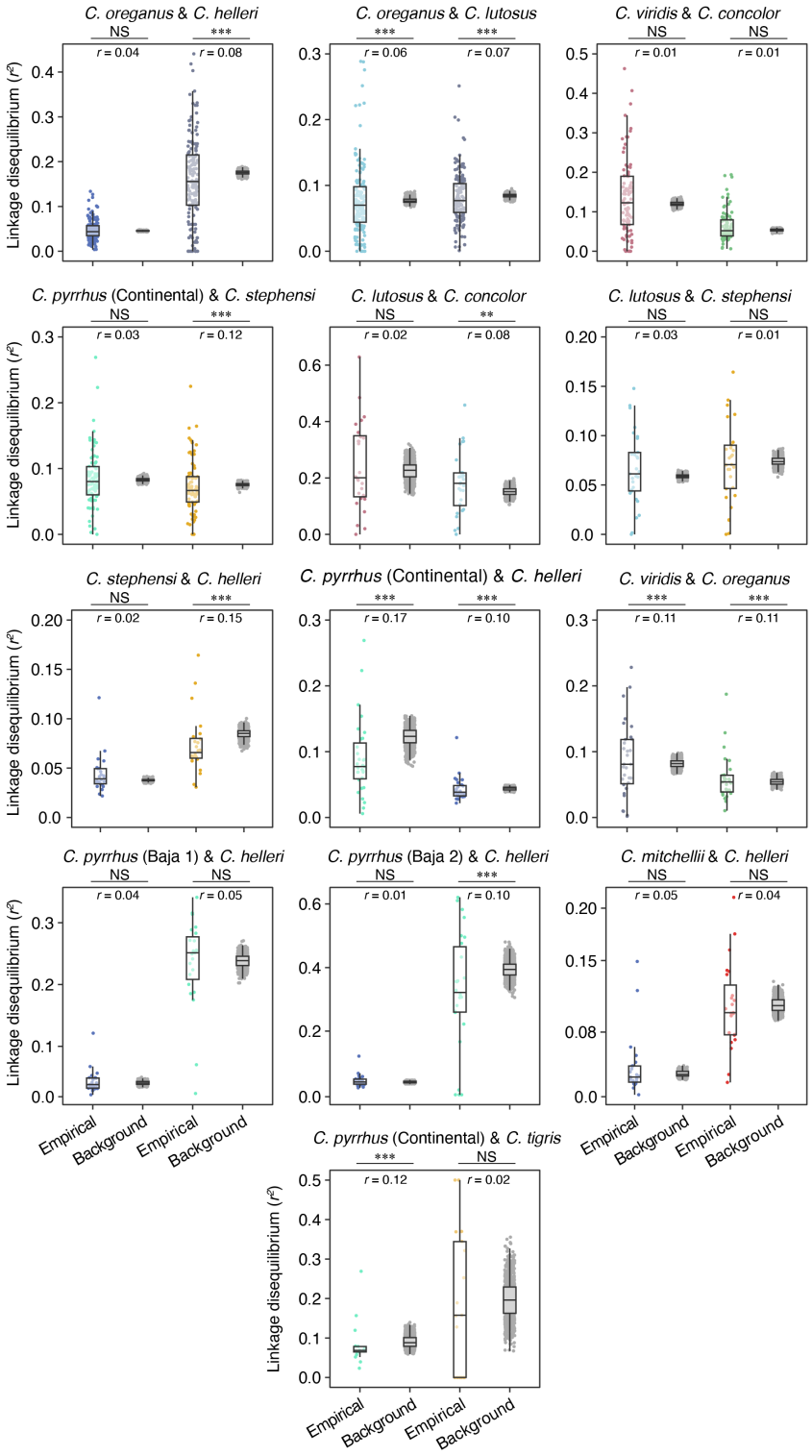

Figure S22. Linkage disequilibrium (r2) in empirical high fd outliers and genomic backgrounds, controlling for recombination rate and allele frequency differences. Effect sizes (*r*) from Mann-Whitney U tests and significance are labeled ($^{***}p < 2.2 \times 10^{-16}$; ** $p < 0.001$; NS, not significant).

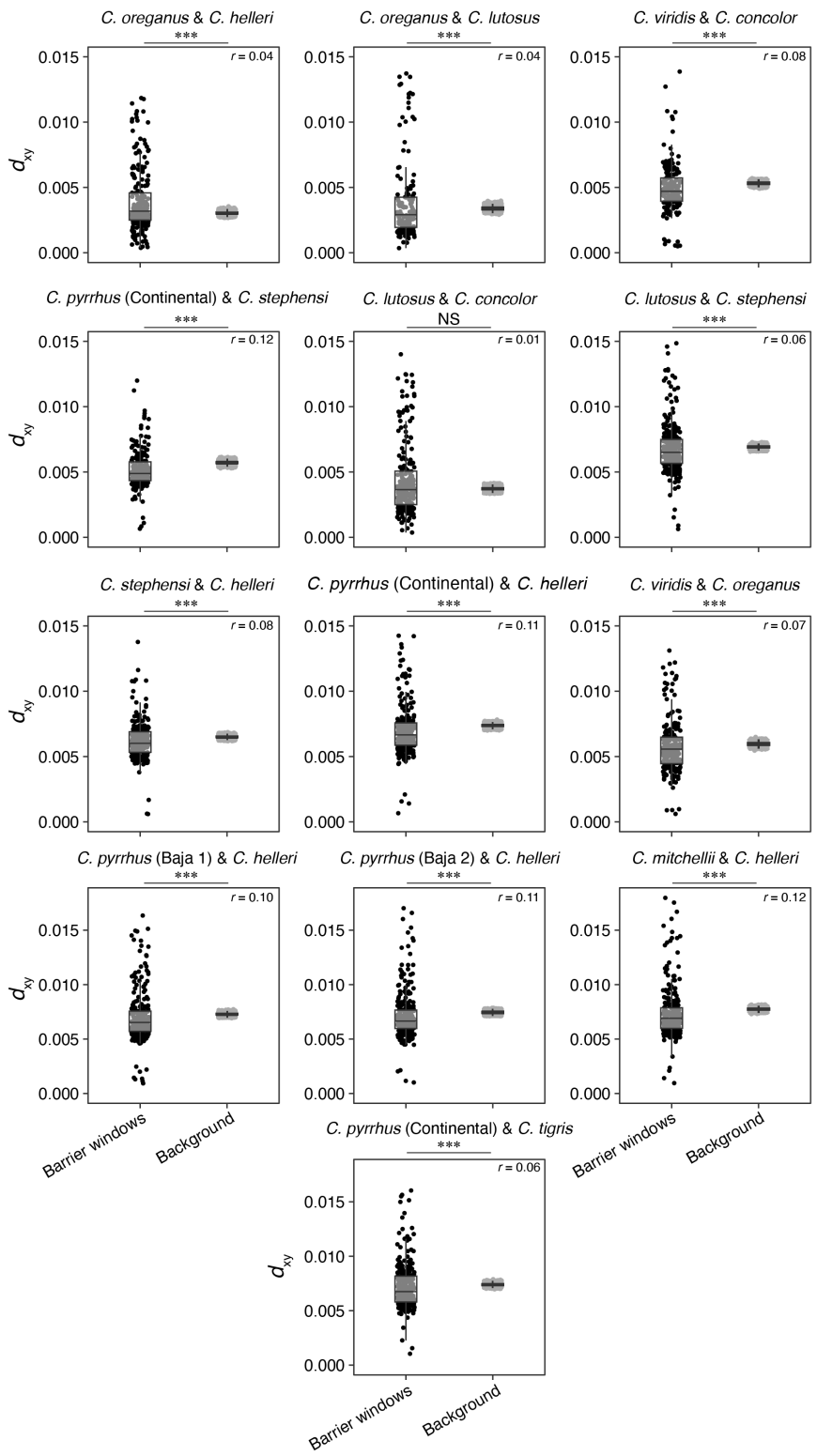

Figure S23. Distributions of d_{xy} in barrier windows and genomic backgrounds for all species pairs analyzed in the study. Effect sizes (r) from Mann-Whitney U tests and significance are labeled ($^{***}p < 2.2 \times 10^{-16}$; NS, not significant).

Tables

Table S1. Summary statistics for the Southwestern Speckled Rattlesnake (*Crotalus pyrrhus*) genome assembly and annotation.

Genome size	1.6 Gbp
Scaffold N50	206.8 Mbp
Scaffold N90	23.1 Mbp
Number of scaffolds	284
Number of gaps	74
Number of N's	7,680 bp
BUSCO completeness	98.43%
Protein-coding genes	19,217
GC content	39%
Repeat content	51%

Table S2. Summary of repeat elements annotated in the *Crotalus pyrrhus* genome using RepeatMasker.

Element family	Number of elements	Length (bp)	Genome %
Retroelements	2,157,807	525,495,056	32.91
SINEs	368,249	42,065,968	2.63
Penelope	26	4,286	0
LINEs	1,327,679	341,049,241	21.36
CRE/SLACS	14	999	0
L2/CR1/Rex	576,798	124,735,680	7.81
R1/LOA/Jockey	9,152	1,451,944	0.09
R2/R4/NeSL	58,117	23,747,228	1.49
RTE/Bov-B	174,860	51,460,250	3.22
L1/CIN4	248,553	78,088,181	4.89
LTR elements	461,879	142,379,847	8.92
BEL/Pao	6,472	2,959,855	0.19
Ty1/Copia	39,897	8,439,539	0.53
Gypsy/DIRS1	245,907	106,318,441	6.66
Retroviral	126,407	17,224,297	1.08
DNA transposons	1,407,197	182,646,711	11.44
hobo-Activator	731,758	98,726,167	6.18
Tc1-IS630-Pogo	322,166	50,306,053	3.15
En-Spm	51	8,704	0
MULE-MuDR	7,078	1,242,179	0.07
PiggyBac	3,080	240,853	0.02
Tourist/Harbinger	105,012	8,601,986	0.54
Other (Mirage, P-element, Transib)	7,510	976,423	0.06
Rolling-circles	30,077	3,087,446	0.19
Unclassified	410,709	66,079,833	4.14
Total interspersed repeats		774,225,886	48.48
Small RNA	38,099	6,797,498	0.43
Satellites	36,514	3,635,169	0.23
Simple repeats	74,965	27,988,561	1.75
Total bases masked		814,207,325	50.98

Table S3. Samples used in the study, collector/museum accessions, and locality data. Precise sampling coordinates are available upon request and are omitted here to protect sensitive populations. Requests can be sent to drew.schield[at]virginia.edu.

Sample	Collector/museum ID	Species	Country	State	County	Reference
CA0346	CAS 229233	*Crotalus atrox*	USA	New Mexico	San Miguel	Schield et al. 2020
CR0001	CAS 223514	*Crotalus ruber*	USA	California	Imperial	Schield et al. 2020
CT10189615	CLP2741	*Crotalus tigris*	USA	Arizona	Santa Cruz	Margres et al. 2021
TR0001	MM109	*Crotalus tigris*	USA	Arizona	Santa Cruz	This study
TR0002	–	*Crotalus tigris*	USA	Arizona	Maricopa	This study
TR0003	–	*Crotalus tigris*	USA	Arizona	Maricopa	This study
TR0004	–	*Crotalus tigris*	USA	Arizona	Maricopa	This study
SR0002	–	*Crotalus stephensi*	USA	California	Inyo	This study
SR0003	–	*Crotalus stephensi*	USA	California	Inyo	This study
SR0004	–	*Crotalus stephensi*	USA	California	Inyo	This study
SR0005	–	*Crotalus stephensi*	USA	California	Inyo	This study
SR0006	–	*Crotalus stephensi*	USA	California	Inyo	This study
SR0007	–	*Crotalus stephensi*	USA	California	Inyo	This study
SR0008	–	*Crotalus stephensi*	USA	California	Inyo	This study
SR0009	–	*Crotalus stephensi*	USA	California	Inyo	This study
SR0010	–	*Crotalus stephensi*	USA	California	Inyo	This study
SR0011	–	*Crotalus stephensi*	USA	California	Inyo	This study
SR0012	–	*Crotalus stephensi*	USA	California	Inyo	This study
SR0013	–	*Crotalus stephensi*	USA	California	Inyo	This study
SR0014	–	*Crotalus stephensi*	USA	California	Inyo	This study
SR0015	–	*Crotalus stephensi*	USA	California	Inyo	This study
SR0019	–	*Crotalus stephensi*	USA	California	Inyo	This study
SR0020	–	*Crotalus stephensi*	USA	California	Inyo	This study
SR0016	–	*Crotalus pyrrhus*	USA	California	San Bernardino	This study
SR0017	–	*Crotalus pyrrhus*	USA	California	San Bernardino	This study
SR0018	–	*Crotalus pyrrhus*	USA	California	San Bernardino	This study
SR0021	–	*Crotalus pyrrhus*	USA	Arizona	Maricopa	This study
SR0022	–	*Crotalus pyrrhus*	USA	Arizona	Maricopa	This study
SR0023	–	*Crotalus pyrrhus*	USA	Arizona	Maricopa	This study
SR0024	–	*Crotalus pyrrhus*	USA	Arizona	Maricopa	This study
SR0025	–	*Crotalus pyrrhus*	USA	Arizona	Maricopa	This study
SR0026	–	*Crotalus pyrrhus*	USA	Arizona	Maricopa	This study
SR0027	–	*Crotalus pyrrhus*	USA	Arizona	Maricopa	This study
SR0028	–	*Crotalus pyrrhus*	USA	Arizona	Maricopa	This study
SR0029	–	*Crotalus pyrrhus*	USA	Arizona	Maricopa	This study
SR0030	–	*Crotalus pyrrhus*	USA	Arizona	Maricopa	This study
SR0031	–	*Crotalus pyrrhus*	USA	Arizona	Maricopa	This study
SR0044	CLP2656	*Crotalus pyrrhus*	Mexico	Baja California	–	This study
SR0049	JLS313	*Crotalus pyrrhus*	Mexico	Baja California	–	This study
SR0053	MM0529	*Crotalus pyrrhus*	Mexico	Baja California	–	This study
SR0054	MM0530	*Crotalus pyrrhus*	Mexico	Baja California	–	This study
SR0055	MM0533	*Crotalus pyrrhus*	Mexico	Baja California	–	This study
SR0078	–	*Crotalus pyrrhus*	USA	Arizona	Maricopa	This study
SR0079	JMM 722	*Crotalus pyrrhus*	Mexico	Baja California	–	This study
SR0080	JMM 723	*Crotalus pyrrhus*	Mexico	Baja California	–	This study
SR0081	JMM 724	*Crotalus pyrrhus*	Mexico	Baja California	–	This study
SR0083	JMM 727	*Crotalus pyrrhus*	Mexico	Baja California	–	This study
SR0086	BGM 834	*Crotalus pyrrhus*	USA	Arizona	Yuma	This study
SR0088	JMM 685	*Crotalus pyrrhus*	USA	Arizona	La Paz	This study
SR0082	JMM 720	*Crotalus angelensis*	Mexico	Baja California	–	This study
SR0041	CLP2646	*Crotalus mitchellii*	Mexico	Baja Calif. Sur	–	This study
SR0042	CLP2647	*Crotalus mitchellii*	Mexico	Baja Calif. Sur	–	This study
SR0043	CLP2648	*Crotalus mitchellii*	Mexico	Baja Calif. Sur	–	This study
SR0045	CLP2657	*Crotalus mitchellii*	Mexico	Baja Calif. Sur	–	This study

Table S3 (continued). Samples used in the study, collector/museum accessions, and locality data. Precise sampling coordinates are available upon request and are omitted here to protect sensitive populations. Requests can be sent to drew.schield[at]virginia.edu.

Sample	Collector/museum ID	Species	Country	State	County	Reference
SR0046	CLPT0667	*Crotalus mitchellii*	Mexico	Baja Calif. Sur	–	This study
SR0047	CLPT0671	*Crotalus mitchellii*	Mexico	Baja Calif. Sur	–	This study
SR0048	JLS300	*Crotalus mitchellii*	Mexico	Baja Calif. Sur	–	This study
SR0050	MM0453	*Crotalus mitchellii*	Mexico	Baja Calif. Sur	–	This study
SR0051	MM0516	*Crotalus mitchellii*	Mexico	Baja Calif. Sur	–	This study
SR0052	MM0519	*Crotalus mitchellii*	Mexico	Baja Calif. Sur	–	This study
SR0056	MM0541	*Crotalus mitchellii*	Mexico	Baja Calif. Sur	–	This study
CV0004	SPM-W09003	*Crotalus viridis*	USA	Colorado	Weld	Schield et al. 2020
CV0006	SPM-W09004	*Crotalus viridis*	USA	Colorado	Weld	Schield et al. 2020
CV0008	SPM-W09002	*Crotalus viridis*	USA	Colorado	Weld	Schield et al. 2020
CV0009	SPM-E08130	*Crotalus viridis*	USA	Colorado	Weld	Schield et al. 2021
CV0010	SPM-W08192	*Crotalus viridis*	USA	Colorado	Weld	Schield et al. 2020
CV0011	SPM-E09067	*Crotalus viridis*	USA	Colorado	Weld	Schield et al. 2020
CV0634	DRS214	*Crotalus viridis*	USA	Colorado	Larimer	Schield et al. 2020
CV0636	DRS151	*Crotalus viridis*	USA	Colorado	Larimer	Schield et al. 2020
CV0696	DRS 324	*Crotalus viridis*	USA	Texas	Jeff Davis	Francioli et al. 2025
CV0697	DRS 377	*Crotalus viridis*	USA	Texas	Jeff Davis	Francioli et al. 2025
CV0853	DRS 422	*Crotalus viridis*	USA	Montana	Chouteau	Schield et al. 2021
CV0854	DRS 423	*Crotalus viridis*	USA	Montana	Chouteau	Schield et al. 2021
CV0856	DRS 425	*Crotalus viridis*	USA	Montana	Chouteau	Schield et al. 2021
CV0857	DRS 426	*Crotalus viridis*	USA	Montana	Chouteau	Gopalan et al. 2024
CV0858	DRS 427	*Crotalus viridis*	USA	Montana	Chouteau	Schield et al. 2022
CV0859	DRS 428	*Crotalus viridis*	USA	Montana	Chouteau	Schield et al. 2022
CV0860	DRS 429	*Crotalus viridis*	USA	Montana	Chouteau	Schield et al. 2021
CV0862	DRS 431	*Crotalus viridis*	USA	Montana	Chouteau	Schield et al. 2022
CV0863	DRS 432	*Crotalus viridis*	USA	Montana	Chouteau	Schield et al. 2022
CV0864	DRS 433	*Crotalus viridis*	USA	Montana	Chouteau	Schield et al. 2022
CV0865	DRS 434	*Crotalus viridis*	USA	Montana	Chouteau	Schield et al. 2021
CV0866	DRS 435	*Crotalus viridis*	USA	Montana	Chouteau	This study
CV0867	DRS 436	*Crotalus viridis*	USA	Montana	Chouteau	Schield et al. 2021
CV0868	DRS 437	*Crotalus viridis*	USA	Montana	Chouteau	Schield et al. 2022
CV0869	DRS 438	*Crotalus viridis*	USA	Montana	Chouteau	Schield et al. 2022
CV0870	DRS 439	*Crotalus viridis*	USA	Montana	Chouteau	Schield et al. 2021
CV0945	RWO034	*Crotalus viridis*	USA	Texas	Jeff Davis	Francioli et al. 2025
CV0946	RWO038	*Crotalus viridis*	USA	Texas	Brewster	This study
CV0947	RWO039	*Crotalus viridis*	USA	Texas	Brewster	Francioli et al. 2025
CV0948	RWO040	*Crotalus viridis*	USA	Texas	Brewster	Francioli et al. 2025
CV0949	RWO041	*Crotalus viridis*	USA	Texas	Brewster	This study
CV0950	RWO042	*Crotalus viridis*	USA	Texas	Brewster	Francioli et al. 2025
CV0951	RWO043	*Crotalus viridis*	USA	Texas	Brewster	Francioli et al. 2025
CV1037	RWO138	*Crotalus viridis*	USA	Texas	Jeff Davis	Francioli et al. 2025
CV1038	RWO139	*Crotalus viridis*	USA	Texas	Brewster	Francioli et al. 2025
CV0985	TAC 332	*Crotalus concolor*	USA	Utah	Duchesne	Gopalan et al. 2024
CV0986	TAC 333	*Crotalus concolor*	USA	Utah	Duchesne	This study
CV0989	TAC 336	*Crotalus concolor*	USA	Utah	Duchesne	This study
CV0990	TAC 337	*Crotalus concolor*	USA	Utah	Duchesne	This study
CV0991	TAC 338	*Crotalus concolor*	USA	Utah	Duchesne	This study
CV1148	TAC 22-01	*Crotalus concolor*	USA	Utah	Duchesne	This study
CV1149	TAC 22-02	*Crotalus concolor*	USA	Utah	Duchesne	This study
CV1150	TAC 22-03	*Crotalus concolor*	USA	Utah	Uintah	This study
CV1151	TAC 22-04	*Crotalus concolor*	USA	Utah	Uintah	This study
CV1152	TAC 22-05	*Crotalus concolor*	USA	Utah	Uintah	This study
CV1153	TAC 22-06	*Crotalus concolor*	USA	Utah	Uintah	This study
CV1154	TAC 22-07	*Crotalus concolor*	USA	Utah	Uintah	This study
CV1227	YZF002	*Crotalus concolor*	USA	Utah	Uintah	This study

Table S3 (continued). Samples used in the study, collector/museum accessions, and locality data. Precise sampling coordinates are available upon request and are omitted here to protect sensitive populations. Requests can be sent to drew.schield[at]virginia.edu.

Sample	Collector/museum ID	Species	Country	State	County	Reference
CV1229	TAC403	*Crotalus concolor*	USA	Utah	Uintah	This study
CV0983	TAC 330	*Crotalus lutosus*	USA	Utah	Beaver	This study
CV0980	TAC 327	*Crotalus lutosus*	USA	Utah	Beaver	This study
CV0982	TAC 329	*Crotalus lutosus*	USA	Utah	Beaver	This study
CV0981	TAC 328	*Crotalus lutosus*	USA	Utah	Beaver	This study
CV0979	TAC 326	*Crotalus lutosus*	USA	Utah	Beaver	This study
CV0988	TAC 335	*Crotalus lutosus*	USA	Utah	Beaver	This study
CV0984	TAC 331	*Crotalus lutosus*	USA	Utah	Beaver	This study
CV0808	DRS 384	*Crotalus lutosus*	USA	Idaho	Ada	This study
CV0809	DRS 385	*Crotalus lutosus*	USA	Idaho	Ada	This study
CV0810	DRS 386	*Crotalus lutosus*	USA	Idaho	Ada	This study
CV0811	DRS 387	*Crotalus lutosus*	USA	Idaho	Ada	This study
CV0812	DRS 388	*Crotalus lutosus*	USA	Idaho	Ada	This study
CV0813	DRS 389	*Crotalus lutosus*	USA	Idaho	Ada	This study
CV0814	DRS 390	*Crotalus lutosus*	USA	Idaho	Ada	This study
CV0815	DRS 391	*Crotalus lutosus*	USA	Idaho	Ada	This study
CV0816	DRS 392	*Crotalus lutosus*	USA	Idaho	Elmore	This study
CV0817	DRS 393	*Crotalus lutosus*	USA	Idaho	Elmore	This study
CV0818	DRS 394	*Crotalus lutosus*	USA	Idaho	Elmore	This study
CV0819	DRS 395	*Crotalus lutosus*	USA	Idaho	Elmore	This study
CV0047	CAS 170423	*Crotalus helleri*	USA	California	San Diego	This study
CV0053	CAS 228044	*Crotalus helleri*	USA	California	San Diego	Bernstein et al. 2025
CV0054	CAS 228048	*Crotalus helleri*	USA	California	San Diego	Bernstein et al. 2025
CV0085	CAS 202983	*Crotalus helleri*	USA	California	Monterey	Schield et al. 2020
CV0086	CAS 205205	*Crotalus helleri*	USA	California	Butte	Bernstein et al. 2025
CV0087	CAS 205756	*Crotalus helleri*	USA	California	Alameda	Schield et al. 2020
CV0093	CAS 206480	*Crotalus helleri*	USA	California	Tulare	Schield et al. 2020
CV0094	CAS 208761	*Crotalus helleri*	USA	California	Fresno	Schield et al. 2020
CV0095	CAS 208762	*Crotalus helleri*	USA	California	Fresno	Schield et al. 2020
CV0096	CAS 208764	*Crotalus helleri*	USA	California	Fresno	Schield et al. 2020
CV0098	CAS 208785	*Crotalus helleri*	USA	California	Fresno	Schield et al. 2020
CV0105	CAS 209200	*Crotalus helleri*	USA	California	Mariposa	Schield et al. 2020
CV0111	CAS 212273	*Crotalus helleri*	USA	California	Fresno	Schield et al. 2019
CV0135	CAS 224764	*Crotalus helleri*	USA	California	Kern	This study
CV0136	CAS 224859	*Crotalus helleri*	USA	California	Fresno	Schield et al. 2020
CV0137	CAS 224926	*Crotalus helleri*	USA	California	Tulare	This study
CV0145	CAS 228193	*Crotalus helleri*	USA	California	Santa Clara	Schield et al. 2020
CV0148	CAS 234626	*Crotalus helleri*	USA	California	Butte	Schield et al. 2020
CV0151	CAS 235855	*Crotalus helleri*	USA	California	Alameda	Schield et al. 2020
CV0152	CAS 236038	*Crotalus helleri*	USA	California	Alameda	Schield et al. 2020
CV0153	CAS 236216	*Crotalus helleri*	USA	California	Kern	Schield et al. 2020
CV0155	CAS 241772	*Crotalus helleri*	USA	California	Alameda	Schield et al. 2020
CV0157	CAS 252894	*Crotalus helleri*	USA	California	Fresno	Schield et al. 2020
CV0158	CAS 252895	*Crotalus helleri*	USA	California	Fresno	This study
CV0159	CAS 252898	*Crotalus helleri*	USA	California	Fresno	This study
CV0160	CAS 252903	*Crotalus helleri*	USA	California	Fresno	This study
CV0161	CAS 253013	*Crotalus helleri*	USA	California	Kern	This study
CV0162	CAS 253041	*Crotalus helleri*	USA	California	Kern	This study
CV0089	CAS 206136	*Crotalus oreganus*	USA	California	Plumas	This study
CV0092	CAS 206280	*Crotalus oreganus*	USA	California	Plumas	This study
CV0101	CAS 208853	*Crotalus oreganus*	USA	California	Mendocino	This study
CV0141	CAS 227633	*Crotalus oreganus*	USA	California	Butte	This study
CV0144	CAS 227703	*Crotalus oreganus*	USA	California	Butte	This study
CV0147	CAS 234623	*Crotalus oreganus*	USA	California	Butte	Bernstein et al. 2025
CV0150	CAS 235854	*Crotalus oreganus*	USA	California	Alameda	Schield et al. 2020

Table S3 (continued). Samples used in the study, collector/museum accessions, and locality data. Precise sampling coordinates are available upon request and are omitted here to protect sensitive populations. Requests can be sent to drew.schield[at]virginia.edu.

Sample	Collector/museum ID	Species	Country	State	County	Reference
CV0764	DRS 333	*Crotalus oreganus*	USA	Idaho	Nez Perce	Schield et al. 2021
CV0083	CAS 172071	*Crotalus oreganus*	USA	Idaho	Nez Perce	Schield et al. 2020
CV0766	DRS 335	*Crotalus oreganus*	USA	Idaho	Nez Perce	Schield et al. 2021
CV0770	DRS 339	*Crotalus oreganus*	USA	Idaho	Nez Perce	Schield et al. 2021
CV0772	DRS 341	*Crotalus oreganus*	USA	Idaho	Nez Perce	Schield et al. 2021
CV0775	DRS 344	*Crotalus oreganus*	USA	Idaho	Nez Perce	Schield et al. 2021
CV0780	DRS 349	*Crotalus oreganus*	USA	Idaho	Nez Perce	Schield et al. 2022
CV0781	DRS 350	*Crotalus oreganus*	USA	Idaho	Nez Perce	Schield et al. 2021
CV0783	DRS 352	*Crotalus oreganus*	USA	Idaho	Nez Perce	Schield et al. 2022
CV0784	DRS 353	*Crotalus oreganus*	USA	Idaho	Nez Perce	Schield et al. 2022
CV0786	DRS 355	*Crotalus oreganus*	USA	Idaho	Nez Perce	Schield et al. 2022
CV0787	DRS 356	*Crotalus oreganus*	USA	Idaho	Nez Perce	Schield et al. 2022
CV0790	DRS 359	*Crotalus oreganus*	USA	Idaho	Nez Perce	Schield et al. 2021
CV0793	DRS 361	*Crotalus oreganus*	USA	Idaho	Nez Perce	Schield et al. 2022
CV0796	DRS 364	*Crotalus oreganus*	USA	Idaho	Nez Perce	Schield et al. 2022
CV0798	DRS 366	*Crotalus oreganus*	USA	Idaho	Nez Perce	Schield et al. 2022
CV0800	DRS 368	*Crotalus oreganus*	USA	Idaho	Nez Perce	Schield et al. 2022

Table S4. Summary of genome-wide introgression between species measured using admixture proportions (f_d), including mean ± standard deviation, median, minimum, and maximum f_d. All summary statistics were calculated using non-overlapping 1 Mb windows across the genome. The standard deviation of f_d for each comparison is indicated in parentheses in the mean column.

Comparison	Mean f_d	Median f_d	Minimum f_d	Maximum f_d
C. oreganus & *C. helleri*	0.245 ± 0.14	0.228	0.001	0.882
C. oreganus & *C. lutosus*	0.224 ± 0.12	0.212	0.001	0.735
C. viridis & *C. concolor*	0.101 ± 0.08	0.087	0	0.638
C. pyrrhus (continental) & *C. stephensi*	0.059 ± 0.06	0.039	0	0.392
C. lutosus & *C. stephensi*	0.045 ± 0.04	0.037	0	0.523
C. lutosus & *C. concolor*	0.051 ± 0.06	0.033	0	0.459
C. stephensi & *C. helleri*	0.030 ± 0.04	0.019	0	0.649
C. pyrrhus (continental) & *C. helleri*	0.027 ± 0.03	0.017	0	0.341
C. viridis & *C. oreganus*	0.024 ± 0.04	0.016	0	0.406
C. pyrrhus (Baja 1) & *C. helleri*	0.022 ± 0.03	0.015	0	0.404
C. mitchellii & *C. helleri*	0.019 ± 0.02	0.013	0	0.184
C. pyrrhus (Baja 2) & *C. helleri*	0.020 ± 0.02	0.013	0	0.332
C. pyrrhus (continental) & *C. tigris*	0.015 ± 0.02	0.01	0	0.22

Table S5. Mean ± standard deviation f_d between species pairs across macrochromsomes, microchromosomes, and the Z chromosome. FDR-corrected *P*-values from Mann-Whitney ∪ tests comparing distributions on different chromosomes are noted in the right column; NS = not significant. All statistics were calculated based on f_d measured in non-overlapping 1 Mb windows.

Species	Mean f_d (macro)	Mean f_d (micro)	Mean f_d (Z)	*P*-value
C. pyrrhus (continental) & *C. stephensi*	0.053 ± 0.05	0.072 ± 0.05	0.033 ± 0.06	macro vs micro (3.9×10^{-5}) macro vs Z (1.4×10^{-10}) micro vs Z (5.9×10^{-11})
C. pyrrhus (continental) & *C. tigris*	0.014 ± 0.02	0.018 ± 0.02	0.008 ± 0.01	macro vs micro (9×10^{-3}) macro vs Z (1.1×10^{-8}) micro vs Z (8.4×10^{-8})
C. lutosus & *C. concolor*	0.055 ± 0.06	0.037 ± 0.03	0.030 ± 0.04	macro vs micro (NS) macro vs Z (1×10^{-2}) micro vs Z (NS)
C. lutosus & *C. stephensi*	0.043 ± 0.03	0.055 ± 0.04	0.032 ± 0.08	macro vs micro (1.5×10^{-4}) macro vs Z (3.5×10^{-9}) micro vs Z (1.5×10^{-9})
C. mitchellii & *C. helleri*	0.018 ± 0.02	0.021 ± 0.02	0.014 ± 0.03	macro vs micro (1.1×10^{-2}) macro vs Z (2×10^{-5}) micro vs Z (2.1×10^{-5})
C. oreganus & *C. helleri*	0.248 ± 0.14	0.218 ± 0.14	0.295 ± 0.2	macro vs micro (7×10^{-3}) macro vs Z (NS) micro vs Z (1.1×10^{-2})
C. oreganus & *C. lutosus*	0.231 ± 0.12	0.199 ± 0.09	0.164 ± 0.14	macro vs micro (5×10^{-3}) macro vs Z (2×10^{-5}) micro vs Z (2×10^{-3})
C. pyrrhus (Baja 1) & *C. helleri*	0.021 ± 0.02	0.025 ± 0.02	0.011 ± 0.02	macro vs micro (NS) macro vs Z (7.5×10^{-8}) micro vs Z (2.3×10^{-7})
C. pyrrhus (Baja 2) & *C. helleri*	0.019 ± 0.02	0.022 ± 0.02	0.010 ± 0.02	macro vs micro (3.8×10^{-2}) macro vs Z (5.8×10^{-8}) micro vs Z (1.9×10^{-7})
C. pyrrhus (continental) & *C. helleri*	0.024 ± 0.03	0.030 ± 0.03	0.020 ± 0.04	macro vs micro (1.6×10^{-2}) macro vs Z (1×10^{-5}) micro vs Z (1.1×10^{-5})
C. stephensi & *C. helleri*	0.026 ± 0.03	0.036 ± 0.03	0.013 ± 0.02	macro vs micro (2.2×10^{-4}) macro vs Z (7.3×10^{-7}) micro vs Z (2.4×10^{-8})
C. viridis & *C. concolor*	0.098 ± 0.08	0.114 ± 0.07	0.035 ± 0.13	macro vs micro (9×10^{-4}) macro vs Z (2.3×10^{-7}) micro vs Z (2×10^{-7})
C. viridis & *C. oreganus*	0.025 ± 0.02	0.021 ± 0.03	0.034 ± 0.07	macro vs micro (NS) macro vs Z (NS) micro vs Z (NS)

Table S6. Mean ± standard deviation F_{ST} between species pairs across macrochromsomes, microchromosomes, and the Z chromosome. FDR-corrected *P*-values from Mann-Whitney ∪ tests comparing distributions on different chromosomes are noted in the right column; NS = not significant. All statistics were calculated based on F_{ST} measured in non-overlapping 1 Mb windows.

Species	Mean F_{ST} (macro)	Mean F_{ST} (micro)	Mean F_{ST} (Z)	*P*-value
C. pyrrhus (continental) & *C. stephensi*	0.682 ± 0.1	0.657 ± 0.11	0.743 ± 0.18	macro vs micro (7.8×10^{-4}) macro vs Z (2.2×10^{-16}) micro vs Z (2.9×10^{-12})
C. pyrrhus (continental) & *C. tigris*	0.800 ± 0.07	0.789 ± 0.08	0.850 ± 0.08	macro vs Z (2.2×10^{-16}) micro vs Z (9.1×10^{-11})
C. lutosus & *C. concolor*	0.483 ± 0.08	0.502 ± 0.05	0.475 ± 0.11	macro vs micro (NS) macro vs Z (NS) micro vs Z (NS)
C. lutosus & *C. stephensi*	0.685 ± 0.1	0.643 ± 0.12	0.767 ± 0.2	macro vs micro (8.2×10^{-7}) macro vs Z (2.2×10^{-16}) micro vs Z (9.2×10^{-12})
C. mitchellii & *C. helleri*	0.648 ± 0.08	0.610 ± 0.1	0.735 ± 0.1	macro vs micro (1.7×10^{-8}) macro vs Z (2.2×10^{-16}) micro vs Z (9.1×10^{-11})
C. oreganus & *C. helleri*	0.113 ± 0.03	0.100 ± 0.03	0.121 ± 0.05	macro vs micro (2×10^{-8}) macro vs Z (6×10^{-3}) micro vs Z (NS)
C. oreganus & *C. lutosus*	0.325 ± 0.09	0.353 ± 0.07	0.458 ± 0.13	macro vs micro (4.9×10^{-5}) macro vs Z (9.5×10^{-15}) micro vs Z (8.4×10^{-10})
C. pyrrhus (Baja 1) & *C. helleri*	0.636 ± 0.1	0.581 ± 0.12	0.752 ± 0.12	macro vs micro (4.9×10^{-9}) macro vs Z (2.2×10^{-16}) micro vs Z (1.3×10^{-12})
C. pyrrhus (Baja 2) & *C. helleri*	0.642 ± 0.1	0.593 ± 0.11	0.766 ± 0.08	macro vs micro (2.6×10^{-8}) macro vs Z (1.1×10^{-16}) micro vs Z (1.0×10^{-12})
C. pyrrhus (continental) & *C. helleri*	0.678 ± 0.11	0.612 ± 0.12	0.786 ± 0.09	macro vs micro (1.3×10^{-9}) macro vs Z (1.3×10^{-16}) micro vs Z (8.7×10^{-14})
C. stephensi & *C. helleri*	0.610 ± 0.15	0.519 ± 0.16	0.740 ± 0.18	macro vs micro (1.8×10^{-9}) macro vs Z (1.4×10^{-16}) micro vs Z (2.5×10^{-12})
C. viridis & *C. concolor*	0.564 ± 0.09	0.530 ± 0.1	0.684 ± 0.16	macro vs micro (4.0×10^{-9}) macro vs Z (1.6×10^{-16}) micro vs Z (1.8×10^{-15})
C. viridis & *C. oreganus*	0.564 ± 0.08	0.526 ± 0.08	0.681 ± 0.15	macro vs micro (1.1×10^{-8}) macro vs Z (4.1×10^{-15}) micro vs Z (5.3×10^{-13})

Table S7. Numbers of recombination hotspots identified in the *Crotalus pyrrhus, C. stephensi, C. oreganus*, and *C. viridis* using different relative heat thresholds and block penalty parameter settings.

Block penalty	Relative heat > 5	Relative heat > 10
Crotalus pyrrhus		
10	4,265	1,713
20	2,052	721
Crotalus stephensi		
10	10,556	4,705
Crotalus oreganus		
10	13,801	6,058
Crotalus viridis		
10	11,026	4,083

Table S8. Mean ± standard deviation f_d in recombination hotspots and coldspots for each species pair and FDR-corrected *P*-values from Mann-Whitney ∪ tests.

Species	f_d in hotspot windows	f_d in coldspot windows	*P*-value
C. pyrrhus (continental) & *C. stephensi*	0.12 ± 0.11	0.07 ± 0.06	$< 2.2 \times 10^{-16}$
C. pyrrhus (continental) & *C. tigris*	0.04 ± 0.03	0.03 ± 0.02	1.2×10^{-16}
C. lutosus & *C. concolor*	0.10 ± 0.09	0.10 ± 0.10	0.3
C. lutosus & *C. stephensi*	0.10 ± 0.08	0.08 ± 0.07	1.5×10^{-11}
C. mitchellii & *C. helleri*	0.05 ± 0.05	0.03 ± 0.02	$< 2.2 \times 10^{-16}$
C. oreganus & *C. helleri*	0.3 ± 0.18	0.32 ± 0.2	4.9×10^{-4}
C. oreganus & *C. lutosus*	0.28 ± 0.17	0.18 ± 0.17	0.8
C. pyrrhus (Baja 1) & *C. helleri*	0.05 ± 0.05	0.04 ± 0.03	1.5×10^{-15}
C. pyrrhus (Baja 2) & *C. helleri*	0.05 ± 0.04	0.03 ± 0.02	9.8×10^{-14}
C. pyrrhus (continental) & *C. helleri*	0.06 ± 0.05	0.04 ± 0.03	$< 2.2 \times 10^{-16}$
C. stephensi & *C. helleri*	0.07 ± 0.06	0.04 ± 0.03	$< 2.2 \times 10^{-16}$
C. viridis & *C. concolor*	0.15 ± 0.13	0.13 ± 0.12	4.2×10^{-11}
C. viridis & *C. oreganus*	0.05 ± 0.04	0.04 ± 0.03	1.3×10^{-11}

Table S9. Mean ± standard deviation f_d in genic and intergenic for each species pair and FDR-corrected *P*-values from Mann-Whitney ∪ tests.

Species	f_d in genic regions	f_d in intergenic regions	*P*-value
C. pyrrhus (continental) & *C. stephensi*	0.094 ± 0.11	0.067 ± 0.08	4.5×10^{-15}
C. pyrrhus (continental) & *C. tigris*	0.034 ± 0.04	0.027 ± 0.03	8.8×10^{-4}
C. lutosus & *C. concolor*	0.101 ± 0.11	0.113 ± 0.13	0.48
C. lutosus & *C. stephensi*	0.085 ± 0.09	0.077 ± 0.08	1.29×10^{-3}
C. mitchellii & *C. helleri*	0.040 ± 0.05	0.036 ± 0.04	8.0×10^{-3}
C. oreganus & *C. helleri*	0.311 ± 0.19	0.317 ± 0.2	0.54
C. oreganus & *C. lutosus*	0.275 ± 0.18	0.164 ± 0.2	0.20
C. pyrrhus (Baja 1) & *C. helleri*	0.049 ± 0.05	0.042 ± 0.05	7.0×10^{-4}
C. pyrrhus (Baja 2) & *C. helleri*	0.043 ± 0.05	0.042 ± 0.04	2.66×10^{-3}
C. pyrrhus (continental) & *C. helleri*	0.054 ± 0.06	0.045 ± 0.05	7.83×10^{-5}
C. stephensi & *C. helleri*	0.062 ± 0.08	0.049 ± 0.06	2.31×10^{-6}
C. viridis & *C. concolor*	0.148 ± 0.14	0.127 ± 0.14	1.22×10^{-9}
C. viridis & *C. oreganus*	0.048 ± 0.05	0.043 ± 0.05	8.76×10^{-4}

Table S10. Results of partial redundancy analysis across species pairs to determine the relative amount of variance in f_d explained by recombination rate and exon density.

Species	Variance explained (recombination rate)	Variance explained (exon density)
C. pyrrhus (continental) & *C. stephensi*	0.09	0.01
C. pyrrhus (continental) & *C. tigris*	0.05	0.0003
C. lutosus & *C. concolor*	0.0004	0.01
C. lutosus & *C. stephensi*	0.05	0.02
C. mitchellii & *C. helleri*	0.04	0.002
C. oreganus & *C. helleri*	0.02	0.01
C. oreganus & *C. lutosus*	0.001	0.0001
C. pyrrhus (Baja 1) & *C. helleri*	0.05	0.01
C. pyrrhus (Baja 2) & *C. helleri*	0.04	0.01
C. pyrrhus (continental) & *C. helleri*	0.06	0.006
C. stephensi & *C. helleri*	0.07	0.008
C. viridis & *C. concolor*	0.008	0.02
C. viridis & *C. oreganus*	0.002	0.001

Table S11. β coefficients and *P*-values (in parentheses) for model terms in linear regression models testing the interaction between recombination rate and exon density, following the formula $f_d \sim$ rate + density + rate × density.

Species	β (rate)	β (density)	β (rate × density)
C. pyrrhus (continental) & *C. stephensi*	5.75×10^{5} (2.2×10^{-16})	3.10×10^{-1} (0.02)	-4.45×10^{6} (0.002)
C. pyrrhus (continental) & *C. tigris*	1.34×10^{5} (1.4×10^{-10})	1.01×10^{-2} (0.81)	-1.21×10^{6} (0.01)
C. lutosus & *C. concolor*	-7.27×10^{4} (0.41)	-5.28×10^{-1} (0.005)	2.93×10^{6} (0.22)
C. lutosus & *C. stephensi*	2.83×10^{5} (4.6×10^{-12})	2.65×10^{-1} (0.004)	-2.15×10^{6} (0.03)
C. mitchellii & *C. helleri*	1.47×10^{5} (4.3×10^{-9})	6.82×10^{-2} (0.22)	-1.43×10^{6} (0.01)
C. oreganus & *C. helleri*	-9.52×10^{5} (6.9×10^{-11})	-1.31×10^{-1} (1.0×10^{-3})	1.42×10^{7} (2×10^{-4})
C. oreganus & *C. lutosus*	-2.52×10^{5} (0.03)	-3.68×10^{-1} (0.18)	5.59×10^{6} (0.07)
C. pyrrhus (Baja 1) & *C. helleri*	4.73×10^{5} (4.9×10^{-10})	9.38×10^{-2} (0.12)	-1.4×10^{6} (0.02)
C. pyrrhus (Baja 2) & *C. helleri*	1.64×10^{5} (4.3×10^{-10})	9.51×10^{-2} (0.09)	-1.53×10^{6} (0.01)
C. pyrrhus (continental) & *C. helleri*	2.77×10^{5} (2.2×10^{-14})	1.65×10^{-1} (0.04)	-2.74×10^{6} (9×10^{-4})
C. stephensi & *C. helleri*	3.72×10^{5} (2.2×10^{-16})	3.35×10^{-1} (4.3×10^{-4})	-5.1×10^{6} (5.2×10^{-8})
C. viridis & *C. concolor*	2.74×10^{5} (0.001)	6.1×10^{-1} (0.001)	-2.7×10^{6} (0.2)
C. viridis & *C. oreganus*	6.79×10^{4} (0.06)	9.39×10^{-2} (0.27)	-1.33×10^{6} (0.3)

Table S12. Spearman correlation coefficients (ρ) and FDR-corrected *P*-values testing relationships between f_d and recombination rate in recombination hotspots.

Species	ρ	*P*-value
C. pyrrhus (continental) & *C. stephensi*	0.36	1.91×10^{-14}
C. pyrrhus (continental) & *C. tigris*	0.21	6.09×10^{-5}
C. lutosus & *C. concolor*	-0.11	8.49×10^{-3}
C. lutosus & *C. stephensi*	0.21	4.81×10^{-8}
C. mitchellii & *C. helleri*	0.15	1.87×10^{-4}
C. oreganus & *C. helleri*	-0.15	1.58×10^{-4}
C. oreganus & *C. lutosus*	-0.02	0.27
C. pyrrhus (Baja 1) & *C. helleri*	0.19	8.14×10^{-5}
C. pyrrhus (Baja 2) & *C. helleri*	0.17	1.87×10^{-4}
C. pyrrhus (continental) & *C. helleri*	0.16	2.72×10^{-4}
C. stephensi & *C. helleri*	0.23	3.84×10^{-5}
C. viridis & *C. concolor*	0.1	0.0137
C. viridis & *C. oreganus*	0.15	8.71×10^{-5}

Table S13. β coefficients and *P*-values for linear regression models testing the relationship between f_d and exon density while controlling for recombination rate in associated hotspots and the physical distance (bp) to the nearest hotspot, following the formula $f_d \sim$ density + rate + distance. *P*-values for each term are indicated in parentheses.

Species	Exon density	Hotspot recombination rate	Distance (bp) to hotspot
C. pyrrhus (continental) & *C. stephensi*	2.02×10^{-1} (0.18)	1×10^{5} (1.8×10^{-11})	-6×10^{-8} (0.42)
C. pyrrhus (continental) & *C. tigris*	-8.5×10^{-3} (0.91)	2.04×10^{4} (4.4×10^{-4})	-1.22×10^{-8} (0.61)
C. lutosus & *C. concolor*	-3.3×10^{-1} (0.1)	-3.4×10^{4} (0.12)	-3.5×10^{-9} (0.9)
C. lutosus & *C. stephensi*	1.8×10^{-1} (0.052)	4.4×10^{4} (2.7×10^{-5})	-5.1×10^{-8} (0.2)
C. mitchellii & *C. helleri*	-3.4×10^{-2} (0.7)	2.5×10^{4} (1.5×10^{-3})	-4×10^{-8} (0.15)
C. oreganus & *C. helleri*	-4.8×10^{-1} (0.15)	-9.8×10^{4} (5.3×10^{-3})	6.2×10^{-8} (0.7)
C. oreganus & *C. lutosus*	-2.1×10^{-1} (0.5)	-2.5×10^{4} (0.48)	-1.1×10^{-7} (0.3)
C. pyrrhus (Baja 1) & *C. helleri*	1.2×10^{-2} (0.91)	3×10^{4} (1.5×10^{-3})	-5.9×10^{-8} (0.1)
C. pyrrhus (Baja 2) & *C. helleri*	7.8×10^{-3} (0.9)	2.3×10^{4} (5.3×10^{-3})	-5.8×10^{-8} (5.0×10^{-2})
C. pyrrhus (continental) & *C. helleri*	5.5×10^{-2} (0.68)	3.1×10^{4} (8.8×10^{-3})	-8.2×10^{-8} (6.6×10^{-2})
C. stephensi & *C. helleri*	3.7×10^{-2} (0.84)	4.7×10^{4} (8.5×10^{-4})	-1.1×10^{-7} (5.0×10^{-2})
C. viridis & *C. concolor*	2.8×10^{-1} (0.12)	3.3×10^{4} (0.14)	-2.5×10^{-8} (0.82)
C. viridis & *C. oreganus*	-3.2×10^{-2} (0.82)	3.6×10^{4} (4.9×10^{-4})	-6.8×10^{-9} (0.90)

Table S14. Results of model testing to evaluate linear versus non-linear relationships between introgression, recombination rate, and divergence across species pairs.

Model	R^2	AICc	*P*-value
Evolutionary divergence ($\rho(f_d \sim$ recombination rate) ~ evolutionary divergence)			
Linear	0.45	-8.31	0.01
Quadratic	0.81	-18.12	0.0002
Evolutionary divergence ($f_d \sim$ evolutionary divergence)			
Linear	0.44	-29.25	0.01
Exponential	0.57	-41.12	0.001
Ecological divergence ($f_d \sim$ ecological divergence)			
Linear	0.38	-28.40	0.02
Exponential	0.32	-27.12	0.06

Table S15. Spearman correlation coefficients (ρ) and FDR-corrected *P*-values testing relationships between genome-wide f_d landscapes of independent species pairs.

f_d landscape 1	f_d landscape 2	ρ	*P*-value
C. oreganus & *C. helleri*	*C. viridis* & *C. concolor*	-0.143	3.62×10^{-6}
C. oreganus & *C. helleri*	*C. pyrrhus* (continental) & *C. stephensi*	-0.16	7.86×10^{-7}
C. oreganus & *C. helleri*	*C. lutosus* & *C. concolor*	0.053	0.232
C. oreganus & *C. helleri*	*C. lutosus* & *C. stephensi*	-0.134	7.26×10^{-5}
C. oreganus & *C. helleri*	*C. pyrrhus* (continental) & *C. tigris*	-0.042	0.293
C. oreganus & *C. lutosus*	*C. viridis* & *C. concolor*	0.268	2.54×10^{-19}
C. oreganus & *C. lutosus*	*C. pyrrhus* (continental) & *C. stephensi*	-0.024	0.525
C. oreganus & *C. lutosus*	*C. stephensi* & *C. helleri*	0.043	0.298
C. oreganus & *C. lutosus*	*C. pyrrhus* (continental) & *C. helleri*	0.074	0.047
C. oreganus & *C. lutosus*	*C. pyrrhus* (Baja 1) & *C. helleri*	0.072	0.047
C. oreganus & *C. lutosus*	*C. pyrrhus* (Baja 2) & *C. helleri*	0.083	0.031
C. oreganus & *C. lutosus*	*C. mitchelli* & *C. helleri*	0.049	0.232
C. oreganus & *C. lutosus*	*C. pyrrhus* (continental) & *C. tigris*	-0.008	0.838
C. viridis & *C. concolor*	*C. pyrrhus* (continental) & *C. stephensi*	0.154	2.67×10^{-6}
C. viridis & *C. concolor*	*C. lutosus* & *C. stephensi*	0.193	3.12×10^{-8}
C. viridis & *C. concolor*	*C. stephensi* & *C. helleri*	0.194	6.25×10^{-7}
C. viridis & *C. concolor*	*C. pyrrhus* (continental) & *C. helleri*	0.202	8.13×10^{-8}
C. viridis & *C. concolor*	*C. pyrrhus* (Baja 1) & *C. helleri*	0.203	9.78×10^{-8}
C. viridis & *C. concolor*	*C. pyrrhus* (Baja 2) & *C. helleri*	0.193	4.51×10^{-7}
C. viridis & *C. concolor*	*C. mitchelli* & *C. helleri*	0.199	2.73×10^{-7}
C. viridis & *C. concolor*	*C. pyrrhus* (continental) & *C. tigris*	0.109	0.004
C. pyrrhus (continental) & *C. stephensi*	*C. lutosus* & *C. concolor*	-0.015	0.759
C. pyrrhus (continental) & *C. stephensi*	*C. viridis* & *C. oreganus*	0.082	0.046
C. pyrrhus (continental) & *C. stephensi*	*C. mitchelli* & *C. helleri*	0.259	9.21×10^{-11}
C. lutosus & *C. concolor*	*C. stephensi* & *C. helleri*	-0.037	0.525
C. lutosus & *C. concolor*	*C. pyrrhus* (continental) & *C. helleri*	0.042	0.45
C. lutosus & *C. concolor*	*C. viridis* & *C. oreganus*	0.026	0.655
C. lutosus & *C. concolor*	*C. pyrrhus* (Baja 1) & *C. helleri*	0.008	0.865
C. lutosus & *C. concolor*	*C. pyrrhus* (Baja 2) & *C. helleri*	-0.016	0.759
C. lutosus & *C. concolor*	*C. mitchelli* & *C. helleri*	-0.017	0.759
C. lutosus & *C. concolor*	*C. pyrrhus* (continental) & *C. tigris*	0.03	0.602
C. lutosus & *C. stephensi*	*C. pyrrhus* (continental) & *C. helleri*	0.183	6.01×10^{-6}
C. lutosus & *C. stephensi*	*C. viridis* & *C. oreganus*	0.084	0.047
C. lutosus & *C. stephensi*	*C. pyrrhus* (Baja 1) & *C. helleri*	0.182	8.11×10^{-6}
C. lutosus & *C. stephensi*	*C. pyrrhus* (Baja 2) & *C. helleri*	0.203	7.86×10^{-7}
C. lutosus & *C. stephensi*	*C. mitchelli* & *C. helleri*	0.181	1.12×10^{-5}
C. lutosus & *C. stephensi*	*C. pyrrhus* (continental) & *C. tigris*	0.096	0.023
C. stephensi & *C. helleri*	*C. viridis* & *C. oreganus*	0.19	3.79×10^{-5}
C. stephensi & *C. helleri*	*C. pyrrhus* (continental) & *C. tigris*	0.225	7.86×10^{-7}
C. pyrrhus (continental) & *C. helleri*	*C. viridis* & *C. oreganus*	0.186	3.73×10^{-5}
C. viridis & *C. oreganus*	*C. pyrrhus* (Baja 1) & *C. helleri*	0.134	0.003
C. viridis & *C. oreganus*	*C. pyrrhus* (Baja 2) & *C. helleri*	0.141	0.003
C. viridis & *C. oreganus*	*C. mitchelli* & *C. helleri*	0.142	0.003
C. viridis & *C. oreganus*	*C. pyrrhus* (continental) & *C. tigris*	0.144	0.001
C. mitchelli & *C. helleri*	*C. pyrrhus* (continental) & *C. tigris*	0.138	0.002

Table S16. Mean ± standard deviation recombination rate in statistical outlier barrier loci compared to the genome background outside of barrier regions for each species pair and FDR-corrected *P*-values from Mann-Whitney ∪ tests.

Species	Barrier loci	Background	*P*-value
C. pyrrhus (continental) & *C. stephensi*	$2.1 \times 10^{-8} \pm 2.6 \times 10^{-8}$	$3.9 \times 10^{-8} \pm 3.8 \times 10^{-8}$	5.8×10^{-10}
C. pyrrhus (continental) & *C. tigris*	$2.4 \times 10^{-8} \pm 2.6 \times 10^{-8}$	$3.6 \times 10^{-8} \pm 3.9 \times 10^{-8}$	4.7×10^{-4}
C. lutosus & *C. concolor*	$3.4 \times 10^{-8} \pm 3.5 \times 10^{-8}$	$3.5 \times 10^{-8} \pm 3.9 \times 10^{-8}$	0.6
C. lutosus & *C. stephensi*	$2.8 \times 10^{-8} \pm 3.8 \times 10^{-8}$	$3.5 \times 10^{-8} \pm 4.1 \times 10^{-8}$	4×10^{-3}
C. mitchellii & *C. helleri*	$2.7 \times 10^{-8} \pm 3.2 \times 10^{-8}$	$3.4 \times 10^{-8} \pm 4.1 \times 10^{-8}$	4×10^{-3}
C. oreganus & *C. helleri*	$4 \times 10^{-8} \pm 4.4 \times 10^{-8}$	$3.2 \times 10^{-8} \pm 3.8 \times 10^{-8}$	1×10^{-3}
C. oreganus & *C. lutosus*	$2.9 \times 10^{-8} \pm 3.8 \times 10^{-8}$	$3.4 \times 10^{-8} \pm 4.0 \times 10^{-8}$	8×10^{-3}
C. pyrrhus (Baja 1) & *C. helleri*	$2.8 \times 10^{-8} \pm 3.6 \times 10^{-8}$	$3.5 \times 10^{-8} \pm 4.0 \times 10^{-8}$	7.8×10^{-5}
C. pyrrhus (Baja 2) & *C. helleri*	$2.7 \times 10^{-8} \pm 3.3 \times 10^{-8}$	$3.5 \times 10^{-8} \pm 4.0 \times 10^{-8}$	4.5×10^{-4}
C. pyrrhus (continental) & *C. helleri*	$2.7 \times 10^{-8} \pm 3.4 \times 10^{-8}$	$3.5 \times 10^{-8} \pm 4.1 \times 10^{-8}$	7.5×10^{-5}
C. stephensi & *C. helleri*	$2.7 \times 10^{-8} \pm 3.7 \times 10^{-8}$	$3.5 \times 10^{-8} \pm 4.1 \times 10^{-8}$	3.5×10^{-5}
C. viridis & *C. concolor*	$2.2 \times 10^{-8} \pm 2.9 \times 10^{-8}$	$3.5 \times 10^{-8} \pm 3.9 \times 10^{-8}$	2.2×10^{-11}
C. viridis & *C. oreganus*	$3 \times 10^{-8} \pm 4.0 \times 10^{-8}$	$3.4 \times 10^{-8} \pm 3.9 \times 10^{-8}$	2×10^{-3}

Table S17. Numbers of shared barrier windows identified on autosomes and the Z chromosome between species pairs, along with FDR-corrected *P*-values from Fisher's exact tests. Shared barrier windows were defined as those identified in more species pairs than would be expected by random chance (see Methods for an explanation of our simulation procedure).

Species	Z barriers	Autosomal barriers	*P*-value
C. pyrrhus (continental) & *C. stephensi*	25	180	4.7×10^{-4}
C. pyrrhus (continental) & *C. tigris*	18	245	0.08
C. lutosus & *C. concolor*	6	226	0.80
C. lutosus & *C. stephensi*	24	250	0.01
C. mitchellii & *C. helleri*	20	230	0.05
C. oreganus & *C. helleri*	15	212	0.37
C. oreganus & *C. lutosus*	24	125	2.04×10^{-6}
C. pyrrhus (Baja 1) & *C. helleri*	22	235	0.02
C. pyrrhus (Baja 2) & *C. helleri*	19	238	0.03
C. pyrrhus (continental) & *C. helleri*	23	234	0.01
C. stephensi & *C. helleri*	22	215	0.03
C. viridis & *C. concolor*	32	163	2.4×10^{-6}
C. viridis & *C. oreganus*	25	205	0.03

Table S18. Mean ± standard deviation f_d in venom genes compared to the genome background and FDR-corrected *P*-values from Mann-Whitney ∪ tests. The genome background for each pair of species was generated using 10,000 random permutations. The *P*-value 'genic' column indicates the FDR-corrected *P*-value from the same test using only genic windows as the genome background.

Species	f_d in venom genes	f_d in genome background	*P*-value	*P*-value genic
C. pyrrhus (continental) & *C. stephensi*	0.10 (0.08)	0.06 (0.01)	0.01	4.3×10^{-4}
C. pyrrhus (continental) & *C. tigris*	0.03 (0.02)	0.02 (0.004)	0.05	2.3×10^{-3}
C. lutosus & *C. concolor*	0.03 (0.02)	0.05 (0.01)	0.95	0.66
C. lutosus & *C. stephensi*	0.05 (0.05)	0.07 (0.01)	0.01	4.3×10^{-4}
C. mitchellii & *C. helleri*	0.03 (0.02)	0.02 (0.01)	0.12	0.10
C. oreganus & *C. helleri*	0.21 (0.11)	0.25 (0.03)	0.95	0.74
C. oreganus & *C. lutosus*	0.24 (0.11)	0.23 (0.02)	0.33	0.19
C. pyrrhus (Baja 1) & *C. helleri*	0.03 (0.01)	0.02 (0.03)	0.12	0.07
C. pyrrhus (Baja 2) & *C. helleri*	0.03 (0.01)	0.02 (0.02)	0.12	0.11
C. pyrrhus (continental) & *C. helleri*	0.04 (0.01)	0.03 (0.03)	0.15	0.06
C. stephensi & *C. helleri*	0.04 (0.01)	0.03 (0.03)	0.31	0.3
C. viridis & *C. concolor*	0.15 (0.04)	0.10 (0.02)	0.03	2.3×10^{-3}
C. viridis & *C. oreganus*	0.05 (0.04)	0.03 (0.01)	0.03	2.3×10^{-3}

Table S19. Mean ± standard deviation f_d in MHC genes compared to the genome background and FDR-corrected *P*-values from Mann-Whitney ∪ tests. The genome background for each pair of species was generated using 10,000 random permutations. The *P*-value 'genic' column indicates the FDR-corrected *P*-value from the same test using only genic windows as the genome background.

Species	f_d in MHC genes	f_d in genome background	*P*-value	*P*-value genic
C. pyrrhus (continental) & *C. stephensi*	0.13 (0.1)	0.06 (0.01)	0.0004	$< 1 \times 10^{-4}$
C. pyrrhus (continental) & *C. tigris*	0.02 (0.01)	0.02 (0.004)	0.36	0.37
C. lutosus & *C. concolor*	0.05 (0.05)	0.05 (0.01)	0.54	0.54
C. lutosus & *C. stephensi*	0.07 (0.05)	0.05 (0.01)	0.02	0.02
C. mitchellii & *C. helleri*	0.05 (0.05)	0.02 (0.03)	0.001	$< 1 \times 10^{-4}$
C. oreganus & *C. helleri*	0.25 (0.12)	0.24 (0.02)	0.51	0.52
C. oreganus & *C. lutosus*	0.20 (0.11)	0.22 (0.01)	0.84	0.85
C. pyrrhus (Baja 1) & *C. helleri*	0.06 (0.05)	0.02 (0.006)	0.003	0.006
C. pyrrhus (Baja 2) & *C. helleri*	0.05 (0.05)	0.02 (0.01)	0.003	0.003
C. pyrrhus (continental) & *C. helleri*	0.07 (0.06)	0.03 (0.01)	$< 1 \times 10^{-4}$	3.3×10^{-4}
C. stephensi & *C. helleri*	0.09 (0.01)	0.03 (0.01)	0.001	0.001
C. viridis & *C. concolor*	0.10 (0.06)	0.10 (0.02)	0.51	0.52
C. viridis & *C. oreganus*	0.07 (0.06)	0.02 (0.01)	$< 1 \times 10^{-4}$	$< 1 \times 10^{-4}$

Table S20. Mean ± standard deviation f_d in spermatogenesis and oogenesis genes compared to the genome background and FDR-corrected *P*-values from Mann-Whitney ∪ tests. The genome background for each pair of species was generated using 10,000 random permutations. The *P*-value 'genic' column indicates the FDR-corrected *P*-value from the same test using only genic windows as the genome background.

Species	f_d in spermatogenesis genes	f_d in genome background	*P*-value	*P*-value genic
C. pyrrhus (continental) & *C. stephensi*	0.04 (0.04)	0.06 (0.01)	0.004	0.003
C. pyrrhus (continental) & *C. tigris*	0.01 (0.01)	0.02 (0.002)	0.001	0.002
C. lutosus & *C. concolor*	0.04 (0.04)	0.05 (0.01)	0.08	0.09
C. lutosus & *C. stephensi*	0.03 (0.03)	0.05 (0.004)	0.0004	0.0002
C. mitchellii & *C. helleri*	0.01 (0.01)	0.02 (0.003)	$< 1 \times 10^{-4}$	$< 1 \times 10^{-4}$
C. oreganus & *C. helleri*	0.28 (0.18)	0.25 (0.02)	0.99	0.99
C. oreganus & *C. lutosus*	0.21 (0.13)	0.22 (0.01)	0.11	0.11
C. pyrrhus (Baja 1) & *C. helleri*	0.01 (0.01)	0.02 (0.004)	$< 1 \times 10^{-4}$	$< 1 \times 10^{-4}$
C. pyrrhus (Baja 2) & *C. helleri*	0.01 (0.01)	0.02 (0.003)	$< 1 \times 10^{-4}$	$< 1 \times 10^{-4}$
C. pyrrhus (continental) & *C. helleri*	0.01 (0.01)	0.03 (0.004)	$< 1 \times 10^{-4}$	$< 1 \times 10^{-4}$
C. stephensi & *C. helleri*	0.01 (0.02)	0.03 (0.005)	3×10^{-3}	$< 1 \times 10^{-4}$
C. viridis & *C. concolor*	0.08 (0.08)	0.10 (0.01)	0.09	0.09
C. viridis & *C. oreganus*	0.02 (0.02)	0.02 (0.004)	0.28	0.28

Table S21. Mean ± standard deviation f_d in embryo development genes compared to the genome background and FDR-corrected *P*-values from Mann-Whitney ∪ tests. The genome background for each pair of species was generated using 10,000 random permutations. The *P*-value 'genic' column indicates the FDR-corrected *P*-value from the same test using only genic windows as the genome background.

Species	f_d in embryo dev. genes	f_d in genome background	*P*-value	*P*-value genic
C. pyrrhus (continental) & *C. stephensi*	0.05 (0.05)	0.06 (0.01)	0.003	$< 1 \times 10^{-4}$
C. pyrrhus (continental) & *C. tigris*	0.01 (0.01)	0.02 (0.002)	0.001	$< 1 \times 10^{-4}$
C. lutosus & *C. concolor*	0.05 (0.06)	0.05 (0.01)	0.88	0.42
C. lutosus & *C. stephensi*	0.04 (0.04)	0.05 (0.01)	0.15	$< 1 \times 10^{-4}$
C. mitchellii & *C. helleri*	0.01 (0.01)	0.02 (0.003)	$< 1 \times 10^{-4}$	$< 1 \times 10^{-4}$
C. oreganus & *C. helleri*	0.29 (0.18)	0.24 (0.02)	1	0.99
C. oreganus & *C. lutosus*	0.22 (0.13)	0.22 (0.01)	0.31	0.30
C. pyrrhus (Baja 1) & *C. helleri*	0.01 (0.01)	0.02 (0.004)	$< 1 \times 10^{-4}$	$< 1 \times 10^{-4}$
C. pyrrhus (Baja 2) & *C. helleri*	0.01 (0.01)	0.02 (0.003)	$< 1 \times 10^{-4}$	$< 1 \times 10^{-4}$
C. pyrrhus (continental) & *C. helleri*	0.01 (0.01)	0.03 (0.01)	$< 1 \times 10^{-4}$	$< 1 \times 10^{-4}$
C. stephensi & *C. helleri*	0.01 (0.01)	0.03 (0.01)	$< 1 \times 10^{-4}$	$< 1 \times 10^{-4}$
C. viridis & *C. concolor*	0.08 (0.06)	0.10 (0.01)	1.4×10^{-4}	0.03
C. viridis & *C. oreganus*	0.02 (0.02)	0.02 (0.005)	$< 1 \times 10^{-4}$	0.02

Table S22. Mean ± standard deviation f_d in oxidative phosphorylation (oxphos) genes compared to the genome background and FDR-corrected *P*-values from Mann-Whitney ∪ tests. The genome background for each pair of species was generated using 10,000 random permutations. The *P*-value 'genic' column indicates the FDR-corrected *P*-value from the same test using only genic windows as the genome background.

Species	f_d in oxphos genes	f_d in genome background	*P*-value	*P*-value genic
C. pyrrhus (continental) & *C. stephensi*	0.05 (0.04)	0.06 (0.01)	0.09	0.08
C. pyrrhus (continental) & *C. tigris*	0.01 (0.01)	0.02 (0.002)	0.04	0.04
C. lutosus & *C. concolor*	0.06 (0.05)	0.05 (0.01)	0.75	0.78
C. lutosus & *C. stephensi*	0.04 (0.03)	0.05 (0.01)	0.34	0.34
C. mitchellii & *C. helleri*	0.01 (0.01)	0.02 (0.003)	$< 1 \times 10^{-4}$	$< 1 \times 10^{-4}$
C. oreganus & *C. helleri*	0.29 (0.17)	0.24 (0.02)	0.99	0.99
C. oreganus & *C. lutosus*	0.22 (0.13)	0.22 (0.01)	0.42	0.44
C. pyrrhus (Baja 1) & *C. helleri*	0.01 (0.01)	0.02 (0.004)	$< 1 \times 10^{-4}$	$< 1 \times 10^{-4}$
C. pyrrhus (Baja 2) & *C. helleri*	0.01 (0.01)	0.02 (0.003)	$< 1 \times 10^{-4}$	$< 1 \times 10^{-4}$
C. pyrrhus (continental) & *C. helleri*	0.01 (0.01)	0.03 (0.01)	$< 1 \times 10^{-4}$	$< 1 \times 10^{-4}$
C. stephensi & *C. helleri*	0.01 (0.01)	0.03 (0.01)	$< 1 \times 10^{-4}$	$< 1 \times 10^{-4}$
C. viridis & *C. concolor*	0.08 (0.06)	0.10 (0.01)	0.03	0.04
C. viridis & *C. oreganus*	0.02 (0.02)	0.02 (0.005)	0.01	0.01

Table S23. Mean ± standard deviation f_d in chemosensory genes compared to the genome background and FDR-corrected *P*-values from Mann-Whitney ∪ tests. The genome background for each pair of species was generated using 10,000 random permutations. The *P*-value 'genic' column indicates the FDR-corrected *P*-value from the same test using only genic windows as the genome background.

Species	f_d in chemosensory genes	f_d in genome background	*P*-value	*P*-value genic
C. pyrrhus (continental) & *C. stephensi*	0.04 (0.05)	0.06 (0.01)	0.04	0.006
C. pyrrhus (continental) & *C. tigris*	0.01 (0.01)	0.02 (0.002)	0.01	0.007
C. lutosus & *C. concolor*	0.05 (0.05)	0.05 (0.01)	0.59	0.46
C. lutosus & *C. stephensi*	0.04 (0.03)	0.05 (0.01)	0.04	0.11
C. mitchellii & *C. helleri*	0.01 (0.01)	0.02 (0.003)	$< 1 \times 10^{-4}$	$< 1 \times 10^{-4}$
C. oreganus & *C. helleri*	0.26 (0.15)	0.24 (0.02)	0.86	0.69
C. oreganus & *C. lutosus*	0.22 (0.13)	0.23 (0.01)	0.42	0.28
C. pyrrhus (Baja 1) & *C. helleri*	0.01 (0.01)	0.02 (0.004)	$< 1 \times 10^{-4}$	$< 1 \times 10^{-4}$
C. pyrrhus (Baja 2) & *C. helleri*	0.01 (0.01)	0.02 (0.003)	$< 1 \times 10^{-4}$	$< 1 \times 10^{-4}$
C. pyrrhus (continental) & *C. helleri*	0.01 (0.01)	0.03 (0.01)	$< 1 \times 10^{-4}$	$< 1 \times 10^{-4}$
C. stephensi & *C. helleri*	0.01 (0.01)	0.03 (0.01)	3×10^{-3}	0.007
C. viridis & *C. concolor*	0.08 (0.06)	0.10 (0.01)	0.04	0.04
C. viridis & *C. oreganus*	0.02 (0.02)	0.03 (0.004)	0.10	0.28

Dataset S1 (separate file). Gene Ontology (GO) terms over/underrepresented in genes within shared barrier loci among Crotalus species, based on homology with Anolis carolinensis gene IDs.

SI References

1. J. M. Meik, J. W. Streicher, A. M. Lawing, O. Flores-Villela, M. K. Fujita, Limitations of climatic data for inferring species boundaries: Insights from speckled rattlesnakes. *PLOS ONE* **10**, e0131435 (2015).

2. J. M. Meik, S. Schaack, O. Flores-Villela, J. W. Streicher, Integrative taxonomy at the nexus of population divergence and speciation in insular speckled rattlesnakes. *J. Nat. Hist.* **52**, 989–1016 (2018).

3. D. R. Schield, *et al.*, Snake recombination landscapes are concentrated in functional regions despite PRDM9. *Mol. Biol. Evol.* **37**, 1272–1294 (2020).

4. J. M. Bernstein, *et al.*, Disentangling a genome-wide mosaic of conflicting phylogenetic signals in Western Rattlesnakes. *Mol. Phylogenet. Evol.* **206**, 108309 (2025).

5. M. L. Holding, M. G. Sovic, T. J. Colston, H. L. Gibbs, The scales of coevolution: comparative phylogeography and genetic demography of a locally adapted venomous predator and its prey. *Biol. J. Linn. Soc.* **132**, 297–317 (2021).

6. D. R. Schield, *et al.*, Allopatric divergence and secondary contact with gene flow: a recurring theme in rattlesnake speciation. *Biol. J. Linn. Soc.* **128**, 149–169 (2019).

7. E. A. Myers, Genome-wide data reveal extensive gene flow during the diversification of the western rattlesnakes (Viperidae: Crotalinae: Crotalus). *Mol. Phylogenet. Evol.* **165**, 107313 (2021).

8. E. A. Myers, *et al.*, Phylogenomic Discordance is Driven by Wide-Spread Introgression and Incomplete Lineage Sorting During Rapid Species Diversification Within Rattlesnakes (Viperidae: *Crotalus* and *Sistrurus*). *Syst. Biol.* **73**, 722–741 (2024).

9. M. E. Douglas, M. R. Douglas, G. W. Schuett, L. W. Porras, Evolution of rattlesnakes (Viperidae; Crotalus) in the warm deserts of western North America shaped by Neogene vicariance and Quaternary climate change. *Mol. Ecol.* **15**, 3353–3374 (2006).

10. D. R. Schield, *et al.*, The roles of balancing selection and recombination in the evolution of rattlesnake venom. *Nat. Ecol. Evol. 2022 69* **6**, 1367–1380 (2022).

11. S. R. Hirst, *et al.*, Where the “ruber” meets the road: Using the genome of the red diamond rattlesnake to unravel the evolutionary processes driving venom evolution. *Genome Biol. Evol.* **16**, evae198 (2024).

12. H. Cheng, G. T. Concepcion, X. Feng, H. Zhang, H. Li, Haplotype-resolved de novo assembly using phased assembly graphs with hifiasm. *Nat. Methods* **18**, 170–175 (2021).

13. N. H. Putnam, *et al.*, Chromosome-scale shotgun assembly using an in vitro method for long-range linkage. *Genome Res.* **26**, 342–350 (2016).

14. H. Li, R. Durbin, Fast and accurate short read alignment with Burrows–Wheeler transform. *Bioinformatics* **25**, 1754–1760 (2009).

15. B. Langmead, S. L. Salzberg, Fast gapped-read alignment with Bowtie 2. *Nat. Methods* **9**, 357–359 (2012).

16. M. Stanke, O. Schöffmann, B. Morgenstern, S. Waack, Gene prediction in eukaryotes with a generalized hidden Markov model that uses hints from external sources. *BMC Bioinformatics* **7**, 62 (2006).

17. M. Stanke, M. Diekhans, R. Baertsch, D. Haussler, Using native and syntenically mapped cDNA alignments to improve de novo gene finding. *Bioinformatics* **24**, 637–644 (2008).

18. A. Smit, R. Hubley, P. Green, RepeatMasker. (2015). Deposited 2015.

19. D. R. Schield, *et al.*, The origins and evolution of chromosomes, dosage compensation, and mechanisms underlying venom regulation in snakes. *Genome Res.* **29**, 590–601 (2019).

20. M. P. Hogan, *et al.*, The genetic regulatory architecture and epigenomic basis for age-related changes in rattlesnake venom. *Proc. Natl. Acad. Sci.* **121**, e2313440121 (2024).

21. C. Jain, S. Koren, A. Dilthey, A. M. Phillippy, S. Aluru, A fast adaptive algorithm for computing whole-genome homology maps. *Bioinformatics* **34**, i748–i756 (2018).

22. M. J. Margres, *et al.*, The tiger rattlesnake genome reveals a complex genotype underlying a simple venom phenotype. *Proc. Natl. Acad. Sci. U. S. A.* **118**, e2014634118 (2021).

23. D. R. Schield, B. W. Perry, Z. L. Nikolakis, S. P. Mackessy, T. A. Castoe, Population Genomic Analyses Confirm Male-Biased Mutation Rates in Snakes. *J. Hered.* **112**, 221–227 (2021).

24. Y. Z. Francioli, *et al.*, Estimation of genome-wide coupling in rattlesnake hybrids provides insight into the process of speciation and its progress. *Nat. Commun.* **16**, 10242 (2025).

25. S. S. Gopalan, *et al.*, Diverse gene regulatory mechanisms alter rattlesnake venom gene expression at fine evolutionary scales. *Genome Biol. Evol.* **16**, evae110 (2024).

26. A. M. Bolger, M. Lohse, B. Usadel, Trimmomatic: a flexible trimmer for Illumina sequence data. *Bioinformatics* **30**, 2114–2120 (2014).

27. A. McKenna, *et al.*, The genome analysis toolkit: A MapReduce framework for analyzing next-generation DNA sequencing data. *Genome Res.* **20**, 1297–1303 (2010).

28. G. A. Van der Auwera, *et al.*, From fastq data to high-confidence variant calls: the genome analysis toolkit best practices pipeline. *Curr. Protoc. Bioinforma.* **43**, 11.10.1-11.10.33 (2013).

29. H. Li, *et al.*, The sequence alignment/map format and SAMtools. *Bioinformatics* **25**, 2078–2079 (2009).

30. D. H. Huson, D. Bryant, The SplitsTree App: interactive analysis and visualization using phylogenetic trees and networks. *Nat. Methods* **21**, 1773–1774 (2024).

31. A. M. Kozlov, D. Darriba, T. Flouri, B. Morel, A. Stamatakis, RAxML-NG: a fast, scalable and user-friendly tool for maximum likelihood phylogenetic inference. *Bioinformatics* **35**, 4453–4455 (2019).

32. A. Stamatakis, RAxML version 8: a tool for phylogenetic analysis and post-analysis of large phylogenies. *Bioinformatics* **30**, 1312–1313 (2014).

33. J. Chifman, L. Kubatko, Quartet Inference from SNP Data Under the Coalescent Model. *Bioinformatics* **30**, 3317–3324 (2014).

34. D. L. Swofford, PAUP*. Phylogenetic Analysis Using Parsimony (*and Other Methods). (2003). Deposited 2003.

35. D. Bryant, V. Moulton, Neighbor-Net: An Agglomerative Method for the Construction of Phylogenetic Networks. *Mol. Biol. Evol.* **21**, 255–265 (2004).

36. S. A. Smith, B. C. O'Meara, treePL: divergence time estimation using penalized likelihood for large phylogenies. *Bioinformatics* **28**, 2689–2690 (2012).

37. T. A. Castoe, C. L. Spencer, C. L. Parkinson, Phylogeographic structure and historical demography of the western diamondback rattlesnake (*Crotalus atrox*): A perspective on North American desert biogeography. *Mol. Phylogenet. Evol.* **42**, 193–212 (2007).

38. X. Zheng, *et al.*, A high-performance computing toolset for relatedness and principal component analysis of SNP data. *Bioinformatics* **28**, 3326–3328 (2012).

39. D. H. Alexander, J. Novembre, K. Lange, Fast model-based estimation of ancestry in unrelated individuals. *Genome Res.* **19**, 1655–1664 (2009).

40. S. Purcell, *et al.*, PLINK: A Tool Set for Whole-Genome Association and Population-Based Linkage Analyses. *Am. J. Hum. Genet.* **81**, 559–575 (2007).

41. J. Terhorst, J. A. Kamm, Y. S. Song, Robust and scalable inference of population history from hundreds of unphased whole genomes. *Nat. Genet.* **49**, 303–309 (2017).

42. S. Schiffels, R. Durbin, Inferring human population size and separation history from multiple genome sequences. *Nat. Genet.* **46**, 919–925 (2014).

43. R. E. Green, *et al.*, Three crocodilian genomes reveal ancestral patterns of evolution among archosaurs. *Science* **346**, 1254449 (2014).

44. J. P. Spence, Y. S. Song, Inference and analysis of population-specific fine-scale recombination maps across 26 diverse human populations. *Sci. Adv.* **5**, eaaw9206 (2019).

45. A. R. Quinlan, I. M. Hall, BEDTools: A flexible suite of utilities for comparing genomic features. *Bioinformatics* **26**, 841–842 (2010).

46. C. Hoge, *et al.*, Patterns of recombination in snakes reveal a tug-of-war between PRDM9 and promoter-like features. *Science* **383**, eadj7026 (2024).

47. S. H. Martin, J. W. Davey, C. D. Jiggins, Evaluating the Use of ABBA–BABA Statistics to Locate Introgressed Loci. *Mol. Biol. Evol.* **32**, 244–257 (2015).

48. R. E. Green, *et al.*, A draft sequence of the Neandertal genome. *Science* **328**, 710–722 (2010).

49. M. Nei, W. H. Li, Mathematical model for studying genetic variation in terms of restriction endonucleases. *Proc. Natl. Acad. Sci.* **76**, 5269–5273 (1979).

50. B. S. Weir, C. C. Cockerham, Esimating F-statistics for the analysis of population structure. *Evolution* **38**, 1358–1370 (1984).

51. K. L. Korunes, K. Samuk, pixy: Unbiased estimation of nucleotide diversity and divergence in the presence of missing data. *Mol. Ecol. Resour.* **21**, 1359–1368 (2021).

52. R Core Team, R: A language and environment for statistical computing. (2020). Deposited 2020.

53. J. B. Pease, M. W. Hahn, More accurate phylogenies inferred from low-recombination regions in the presence of incomplete lineage sorting. *Evolution* **67**, 2376–2384 (2013).

54. P. Danecek, *et al.*, The variant call format and VCFtools. *Bioinformatics* **27**, 2156–2158 (2011).

55. R. J. Hijmans, terra: Spatial Data Analysis. (2025). Deposited 2025.

56. S. E. Fick, R. J. Hijmans, WorldClim 2: new 1-km spatial resolution climate surfaces for global land areas. *Int. J. Climatol.* **37**, 4302–4315 (2017).

57. M. E. Aiello-Lammens, R. A. Boria, A. Radosavljevic, B. Vilela, R. P. Anderson, spThin: an R package for spatial thinning of species occurrence records for use in ecological niche models. *Ecography* **38**, 541–545 (2015).

58. K. G. Ashton, Body size variation among mainland populations of the western rattlesnake (Crotalus viridis). *Evolution* **55**, 2523–2533 (2001).

59. J. Oksanen, *et al.*, vegan: Community Ecology Package. (2016).

60. K. P. Burnham, D. R. Anderson, Multimodel inference: Understanding AIC and BIC in model selection. *Sociol. Methods Res.* **33**, 261–304 (2004).

61. J. Felsenstein, Phylogenies and the Comparative Method. *Am. Nat.* **125**, 1–15 (1985).

62. J. A. Coyne, H. A. Orr, Patterns of Speciation in Drosophila. *Evolution* **43**, 362–381 (1989).

63. H. Mi, A. Muruganujan, D. Ebert, X. Huang, P. D. Thomas, PANTHER version 14: more genomes, a new PANTHER GO-slim and improvements in enrichment analysis tools. *Nucleic Acids Res.* **47**, D419–D426 (2019).

64. J. Alföldi, *et al.*, The genome of the green anole lizard and a comparative analysis with birds and mammals. *Nature* **477**, 587–591 (2011).

65. F. Supek, M. Bošnjak, N. Škunca, T. Šmuc, REVIGO Summarizes and Visualizes Long Lists of Gene Ontology Terms. *PLOS ONE* **6**, e21800 (2011).